IET Generation, Transmission & Distribution

Special issue Call for Papers

Be Seen. Be Cited. Submit your work to a new IET special issue

"Emerging Applications of IoT and Cybersecurity for Electrical Power Systems"

Lead Guest: Editor Mohamed M. F. Darwish
Guest Editors: Mahmoud Elsisi, Diaa-Eldin A. Mansour, Mostafa M. Fouda and Matti Lehtonen

Read more

The Institution of Engineering and Technology

Received: 24 July 2021 | Revised: 13 October 2021 | Accepted: 23 October 2021

IET Generation, Transmission & Distribution

DOI: 10.1049/gtd2.12345

The Institution of Engineering and Technology WILEY

ORIGINAL RESEARCH PAPER

Robust fuzzy model predictive control for voltage regulation in islanded microgrids

Masood Mottaghizadeh[1] | **Farrokh Aminifar**[1] | **Turaj Amraee**[2] | **Majid Sanaye-Pasand**[1]

[1] School of Electrical and Computer Engineering, College of Engineering, University of Tehran, Tehran, Iran

[2] Department of Electrical Engineering, Faculty of Electrical Engineering, K. N. Toosi University of Technology, Tehran, Iran

Correspondence
Farrokh Aminifar, School of Electrical and Computer Engineering, College of Engineering, University of Tehran, Tehran, 11365–4563 Iran.
Email: faminifar@ut.ac.ir

Abstract

An effective robust fuzzy model predictive control (RFMPC) method for secondary voltage control in islanded microgrids (μGs) is presented here. In contrast to the existing techniques, which require a detailed model of μG and an ideal communication network between μG central controller and primary local controllers, RFMPC is synthesized for a non-linear model of the μG with various time delays, uncertainties, and bounded disturbances. The famous Takagi-Sugeno fuzzy approach is adopted to approximate the inherently non-linear model of μG by locally linear dynamics. The Lyapunov–Razumikhin functional method is exploited to deal with time delays. In this regard, sufficient conditions are provided in the form of linear matrix inequalities (LMIs). Then, a sequence of control laws corresponding to a set of terminal constraints is computed offline. Doing so, the online stage is reduced to solving a convex problem with LMI constraints considering the sequence of constraint sets obtained in the offline stage, thereby reducing the computational burden significantly. Robust positive invariance and input-to-state stability property concerning communication network deficiency are then speculated. The effectiveness of the proposed RFMPC is verified via a comprehensive suite of simulations in the MATLAB/SimPowerSystems environment.

1 | INTRODUCTION

Proliferated deployment of distributed energy resources (DERs) along with communication and automation facilities have brought about the concept of microgrid (μG). Depending on the access to the upstream main grid, μG can be operated in either grid-connected or islanded modes. DERs may be interfaced to the grid directly through AC rotating machines or via power electronic converters, say voltage source inverters (VSIs). A standard μG voltage control strategy consists of different hierarchical levels: primary (maintaining the voltage stability of μG by local controllers), secondary (eliminating the voltage deviations stemmed from the operation of primary controllers), and tertiary (tuning the controller setpoints based on economic criteria) [1]. Secondary and tertiary control levels usually have a central architecture.

The main focus of this paper is to propose a secondary voltage control approach in islanded μGs. The objective is to restore the voltage magnitudes of all DERs to their desired values. As an optimal control approach, model predictive control (MPC) belongs to an advanced class of predictive controllers that ended up successful outcomes in both practical and academic domains [2]. Some of the advantages of MPC for μGs are as follows: (1) It is based on an explicit prediction of future μG behaviour; (2) time delays, inherent non-linearities, and changing control objectives can be easily analysed; (3) it enjoys simple and fast implementation; (4) MPC involves straightforward design procedure, which makes it to be more flexible; (5) it can deal with constraints on states and inputs easily, such as maximum control inputs constraints; and (6) MPC explicitly includes constraints on the DERs and takes into account the system dynamics [3, 4].

There exist a number of challenges in the implementation of MPC as a central control technique for the secondary voltage control of μGs. When the data are being transmitted through communication networks from the DERs to the central controller, the communication delay is unavoidable. Communication delay is a practical challenge in the central control paradigm that is overlooked in the majority of studies. Communication

This is an open access article under the terms of the Creative Commons Attribution License, which permits use, distribution and reproduction in any medium, provided the original work is properly cited.
© 2021 The Authors. *IET Generation, Transmission & Distribution* published by John Wiley & Sons Ltd on behalf of The Institution of Engineering and Technology

17518695, 2022, 5, Downloaded from https://ietresearch.onlinelibrary.wiley.com/doi/10.1049/gtd2.12345 by Readcube (Labtiva Inc.), Wiley Online Library on [04/11/2022]. See the Terms and Conditions (https://onlinelibrary.wiley.com/terms-and-conditions) on Wiley Online Library for rules of use; OA articles are governed by the applicable Creative Commons License

delay potentially degrades the system dynamic performance; it can even bring about instability, if not considered properly. In addition, μG parameters, such as line impedances, load values and models, and DERs' parameters are uncertain due to the modelling simplifications, errors in parameter estimation, and unknown phenomena. Besides, classical MPC methods suffer from excessive computation effort. These challenges turn into major barriers when the number of DERs and/or the size of μG grow [5].

A majority of the proposed methodologies have ignored the time delays between the μG central controller and primary local controllers [6, 7]. In [6], a fully centralized finite control set MPC, that restores all voltage magnitudes to their reference values considering minimum convergence rate, was proposed for multiple DERs μG in both grid-connected and islanded modes. Authors in [7] proposed a multi-layer structure for voltage regulation by taking into account the large-signal dynamical model of islanded μGs. The malicious effect of the communication latency on the stability of μGs and how to eliminate the effects of communication delay has been discussed in [8–10]. The time delay may be either constant or random. Reference [8] proposed a robust control scheme for frequency restoration subject to voltage constraints in autonomous μGs in the presence of time-varying and unknown communication delays. In [9], a centralized control scheme that coordinates parallel operations of multiple DERs within a μG was presented, in which the authors utilized a two-step prediction technique to estimate the maximum time delay. In [10], authors utilized the small-signal dynamical model of μG to analyse the stability robustness of secondary voltage control against communication latency, and the delay margin under which the system is stable was calculated.

Authors in [11] presented a predictive control based on modified finite control set for voltage control in islanded μG. This method offers a quick dynamic reaction only when the time delay is considered as a constant value. Generalized predictive control was proposed in [12] that is robust under variable parameters, variable structure, and time-varying delay scenarios. Also, it can handle fixed delay and random delay as well as enhance tracking speed. But this method suffers from a large computation burden and high demand for a mathematical model. In [13], a networked predictive control is proposed to handle both fixed and random delays that can eliminate the need for mathematical models and have high robustness; however, the influence of practical factors, such as network uncertainties, was not analysed. Authors in [14] proposed a method based on MPC to enhance the robustness of secondary control under large time delays. But this method requires a complex algorithm, which leads to low dynamic performance and high computation burden. In order to improve dynamic performance, a linearization approach based on neural network predictive control was proposed in [15]. However, this method was not able to handle any communication delays. Authors in [16] proposed a weighted average predictive control in order to improve consensus convergence and strong anti-interference ability; however, this method suffers from uncertainties, and the random delay was not considered. Authors in [17] proposed a Smith predictor controller that can handle both fixed delay and random communication delays. Although this controller enhanced the dynamic response of MPC, it suffers from external disturbances and model uncertainties.

Another technical concern around the communication networks is that most control methods employed wireless communication networks, such as LTE/4G or Wi-Fi that are exposed to environmental harsh conditions; hence, inevitably introduce noise and disturbances in the network [18]. Author in [19] proposed a centralized statistical method to restore voltage of islanded μGs concerning communication noises and disturbances. In [20], this idea was extended to consider time-varying communication delays and noises concurrently in order to improve the dynamic performance of secondary voltage control in islanded μGs. In [21], an approach based on the Lyapunov function was introduced to establish the stability of the classic MPC, which requires a perfect model μG without disturbances. The key point is to find a Lyapunov function for MPC. In [22], a robust MPC was proposed by considering constrained time-delayed systems with uncertainty descriptions. Authors in [23] proposed a probability-based constrained MPC for systems concerning both uncertainties and time delays, in which random delays were included. In [24], a stochastic MPC is proposed to compensate for the disturbances on the load profile and on the power delivered by DERs that are connected to islanded μG so as to guarantee the fulfillment of the operational constraints. A linear controller in [25] is introduced for keeping the real trajectory close to the reference values and introducing scaling factors for balancing disturbances' compensation from different controllable components of μG, such as DGs, energy storage systems, and loads.

In addition to communication network deficiency, the μG is per se mostly non-linear due to the presence of non-linear equipment, for example, power electronics-interfaced resources. In this regard, some studies employed non-linear methods, such as non-linear MPC (NMPC) proposed for voltage regulation in [26]; however, non-linear methods suffer from high computation burden; as a result, NMPC methods may not able to execute effectively in the real world. To cope with the challenges of the non-linearity of systems, the Takagi-Sugeno (T-S) fuzzy system is a highly favourable alternative [27]. Based on the T-S fuzzy system, the non-linear system can be approximated by several piecewise linear subsystems; thus, linear control methods can be employed for control problems [28]. More recently, the T-S fuzzy model has been exploited in the control of parallel islanded μGs, as reported in [29]; the problem of synchronization in the presence of time-varying communication delay was however left behind. Despite the advantages of T-S fuzzy approaches in the transformation of non-linear dynamics to linear ones, they suffer from low control criteria performances, a longer settling time for instance.

From an economic point of view, the majority of operators in all countries do not pay more attention to their computation systems and utilize traditional ones to reduce their cost, which, in turn, may lead to an increase in the computational burden to a great extent. MPC requires to solve an optimization problem at each sampling time so as to obtain control inputs. In this regard, the more non-linear a system is, the longer the

17518695, 2022, 5, Downloaded from https://ietresearch.onlinelibrary.wiley.com/doi/10.1049/gtd2.12345 by Readcube (Labtiva Inc.), Wiley Online Library on [04/11/2022]. See the Terms and Conditions (https://onlinelibrary.wiley.com/terms-and-conditions) on Wiley Online Library for rules of use; OA articles are governed by the applicable Creative Commons License

computation time is needed. The combination of T-S fuzzy model with MPC can basically support the concurrent realization of the high computational effort of conventional MPC methods and the non-linear dynamic model of μG [30]. The reduction of computational burden and improving control criteria are the most significant superiorities of such methods. Authors in [31] proposed a secondary voltage control based on the combination of fuzzy systems and MPC; however, only fixed delays and low disturbances are considered. The authors in [32] proposed a predictive controller for time-delayed T-S fuzzy systems by taking advantage of the linear matrix inequality (LMI) techniques. Although the non-linear characteristics of μG have been studied in the above-mentioned papers, the appearance of disturbances and model uncertainties, which are ubiquitous in the industrial process, can cause severe degradation of the control performance.

Briefly, the main drawbacks of the reviewed studies are as follows: (1) The majority of existing secondary voltage control methods require a detailed and complete model of μG, which is not achievable in practice; (2) also, they require an ideal communication network between the primary controllers and central controller, which means that they ignore time-varying delays and disturbances in the process of controller design or consider time delay as a constant value; and (3) above all, μGs are naturally non-linear, and the use of non-linear methods to deal with this challenge may impose a heavy burden on controllers alongside the fact that non-linear methods suffer from inaccuracy of parameters.

Motivated by the above challenges and in order to cope with them, in this paper, a robust fuzzy MPC (RFMPC) method capable to deal with time delays, noises, and microgrid operation uncertainties is proposed for the secondary voltage restoration of islanded μGs. The salient novelties of the proposed RFMPC are:

1. An RFMPC method is proposed for islanded μGs confronting uncertainties, disturbances, and time-varying delays simultaneously, which have not been investigated previously.
2. The Lyapunov–Razumikhin functional (LRF) method [33] is utilized to construct a sequence of the terminal constraint set corresponding to a sequence of control laws offline, and sufficient conditions for robust positive invariance (RPI) sets are provided in the form of LMIs. Afterward, an online optimization algorithm is introduced to reduce the computational burden of controller synthesis. All states (current and delayed) of the system are entered into the terminal constraint set at the end of the prediction horizon; and also, the proposed method is input-to-state stable (ISS).
3. The bounded uncertainties and disturbances are wisely captured in the RFMPC. To do so, the objective function of the optimization problem is recast by adding a term addressing the disturbances and uncertainties, and the min-max approach is employed to achieve disturbance rejection property with respect to their maximum values.
4. The majority of reviewed methods focused only on improving the dynamical response of controllers and neglected computation effort, which is a challenging hamper in the real-world applications. Meanwhile, nowadays, due to the privatization of distribution systems, it is attempted to reduce the costs and increase the profit. In this regard, running more complex methods requires updated systems, which can be costly. Consequently, system managers prefer to use undeveloped controllers, which in turn, lead to increase of computation time and reduce controller efficiency. In this paper, we propose a method in order to reduce it by separating the original objective function into offline and online stages. In the offline stage, an optimal convergence region is achieved. Then, the online optimization problem is solved according to the obtained optimal convergence region, which can reduce the computation burden to a great extent. In this paper, we showed that the proposed method can reduce the computation time using the same hardware.
5. For μGs, RFMPC is significantly important since the centralized control is not tractable for large time delays. The proposed RFMPC approach can alleviate time-varying, large communication delays effectively, without threatening the stability of controllers.
6. For the first time, two types of DERs, synchronous and inverter-interfaced ones, are considered in the secondary voltage control of islanded μG, which only inverter-based DERs have been studied previously.

2 | PRELIMINARIES AND SYSTEM MODELING

2.1 | System modelling

A general μG model is composed of the following specific submodels: synchronous DERs, inverter-interfaced DERs, network, and loads. The non-linear large-signal dynamic model of each DER is formulated in its own *d-q* (direct-quadrature) reference frame with respect to its own rotating frequency of ω_i. In order to acquire the overall dynamical model on a uniform frame for μG, the reference frame of one DER is designated as the common *D-Q* reference frame. δ_i is the rotating angle difference (rad) of DER *i* reference frame with respect to the common reference frame which satisfies the following differential equation:

$$\dot{\delta}_i = \omega_i - \omega_{comm} \tag{1}$$

2.1.1 | Dynamic model of synchronous generator

A small-scale synchronous generator is focused here as a study model, Figure 1.

In this paper, the fourth-order non-linear model of the synchronous generator is used for the purpose of voltage regulation. The general form of the non-linear state-space model of

17518695, 2022, 5, Downloaded from https://ietresearch.onlinelibrary.wiley.com/doi/10.1049/gtd2.12345 by Readcube (Labtiva Inc.), Wiley Online Library on [04/11/2022]. See the Terms and Conditions (https://onlinelibrary.wiley.com/terms-and-conditions) on Wiley Online Library for rules of use; OA articles are governed by the applicable Creative Commons License

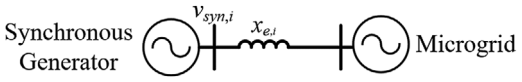

FIGURE 1 Schematic of a small-scale synchronous generator connected to μG

the synchronous generator is as follows [34]:

$$\begin{aligned}\dot{\mathbf{x}}_{syn,i}(t) &= \mathbf{A}_{syn,i}(t)\,\mathbf{x}_{syn,i}(t) + \mathbf{B}_{syn}\mathbf{u}_{syn,i}(t) + \mathbf{D}_{syn}s_{m0,i}\\ \mathbf{y}_{syn,i}(t) &= \mathbf{C}_{syn,i}(t)\mathbf{x}_{syn,i}(t)\end{aligned} \tag{2}$$

where $\mathbf{x}_{syn,i}(t) = [\delta_{syn,i}(t) \quad s_{m,i}(t) \quad e'_{syn,i,q}(t) \quad e'_{syn,i,d}(t)]^T$ is the state vector, $\mathbf{u}_{syn,i}(t) = [\tau_{m,i}(t) \quad v_{fd,i}(t)]^T$ is the control input vector, $\mathbf{y}_{syn,i}(t) = [v_{syn,i,d}(t) \quad v_{syn,i,q}(t)]^T$ is output vector; $e'_{syn,i,d}(t)$, $e'_{syn,i,q}(t)$,$v_{syn,i,d}(t)$, $v_{syn,i,q}(t)$ are direct and quadratic components of transient voltage $e'_{syn,i}(t)$ and output voltage $v_{syn,i}(t)$; $s_{m,i}(t)$ is generator slip; and $\tau_{m,i}(t)$ and $v_{fd,i}(t)$ are the generator control input variables from the excitation and governor systems, respectively.

$$\mathbf{A}_{syn,i}(t) = \begin{bmatrix} 0 & \omega_b & 0 & 0 \\ 0 & a_{22} & a_{23}(t) & a_{24}(t) \\ a_{31}(t) & 0 & a_{33} & 0 \\ a_{41}(t) & 0 & 0 & a_{44} \end{bmatrix}, \quad \mathbf{D}_{syn} = \begin{bmatrix} -1 \\ d_2 \\ 0 \\ 0 \end{bmatrix}$$

$$\mathbf{B}_{syn} = \begin{bmatrix} 0 & 0 \\ b_{21} & 0 \\ 0 & b_{32} \\ 0 & 0 \end{bmatrix}, \quad \mathbf{C}_{syn,i}(t) = \begin{bmatrix} c_{11}(t) & 0 & 0 & c_{14} \\ c_{21}(t) & 0 & c_{23} & 0 \end{bmatrix} \tag{3}$$

In Equation (3), the items a_{22}, a_{33}, d_2, a_{44}, b_{21}, b_{32}, c_{14}, and c_{23} are constant, while the others are non-linear and are defined below:

$$\begin{aligned} a_{23}(t) &= a_{230}\sin\delta_{syn,i}(t) \quad a_{24}(t) = a_{240}\cos\delta_{syn,i}(t)\\ a_{31}(t) &= a_{310}\frac{\cos\delta_{syn,i}(t)}{\delta_{syn,i}(t)} \quad a_{41}(t) = a_{410}\frac{\sin\delta_{syn,i}(t)}{\delta_{syn,i}(t)}\\ c_{11}(t) &= c_{110}\frac{\sin\delta_{syn,i}(t)}{\delta_{syn,i}(t)} \quad c_{21}(t) = c_{210}\frac{\cos\delta_{syn,i}(t)}{\delta_{syn,i}(t)}\end{aligned} \tag{4}$$

The detailed expression of these items can be found in [34]. System (2) is a class of multi-input multi-output (MIMO) nonlinear dynamic systems, in which $\mathbf{A}_{syn,i}(t)$, $\mathbf{C}_{syn,i}(t)$ are functions of the state variable vector $\mathbf{x}_{syn,i}(t)$ and $\mathbf{B}_{syn}$ is a constant matrix.

2.1.2 | Dynamic model of inverter-interfaced DER

The block diagram of an inverter-based DER is illustrated in Figure 2, which consists of the primary energy source, VSI, the series LC filter, and the RL output connector. There are three

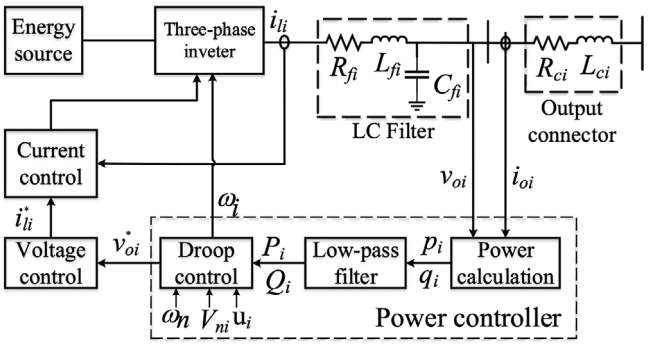

FIGURE 2 Block diagram of an inverter-interfaced DER

control loops in the inverter control scheme: the droop, voltage, and current loops. As analysed in [1], voltage and current loops dynamics can be safely ignored, thereby assuming it as a constant DC voltage source. Hence, we consider the dynamics of the power control loop.

The frequency and voltage droop characteristics for the ith inverter-interfaced DER are presented as:

$$\omega_i = \omega_{ni} - m_{P_i}P_i \tag{5a}$$

$$k_{V_i}\dot{v}_{oi} = V_{ni} - v_{oi} - n_{Q_i}Q_i \tag{5b}$$

where ω_{ni}, V_{ni} are the desired frequency and voltage magnitude; ω_i and v_{oi} represent the output frequency and voltage; k_{V_i} is voltage control gain; m_{P_i} and n_{Q_i} are frequency and voltage droop coefficients; and P_i and Q_i are fundamental components of the output active and reactive powers, respectively. The instantaneous active and reactive powers p_i,q_i are passed through two first-order low-pass filters with the cut-off frequency of ω_{ci}. So, P_i, Q_i are:

$$P_i = \frac{\omega_{ci}}{s + \omega_{ci}}(v_{odi}i_{odi} + v_{oqi}i_{oqi}) \tag{6a}$$

$$Q_i = \frac{\omega_{ci}}{s + \omega_{ci}}(v_{oqi}i_{odi} - v_{odi}i_{oqi}) \tag{6b}$$

where v_{odi}, v_{oqi} and i_{odi}, i_{oqi} represent the d-q axis of output voltage and current of the ith VSI, respectively. The primary voltage control strategy for each DER aligns the output voltage amplitude on the d-axis of the corresponding reference frame. Therefore,

$$k_{V_i}\dot{v}_{odi} = V_{ni} - v_{odi} - n_{Q_i}Q_i + u_{inv,i}, v_{oqi} = 0 \tag{7}$$

therein $u_{inv,i}$ is the secondary voltage control input.

The complete dynamic model of the i^{th} inverter-interfaced DER can be written in a compact form as:

$$\begin{cases} \dot{\mathbf{x}}_{inv,i}(t) = \mathbf{A}_{inv,i}\mathbf{x}_{inv,i}(t) + \mathbf{B}_{inv,i}u_{inv,i}(t) + \mathbf{k}_{inv,i}\mathbf{D}_{inv} \\ \mathbf{y}_{inv,i}(t) = v_{odi} = \mathbf{C}_{inv,i}\mathbf{x}_{inv,i}(t) \end{cases} \tag{8}$$

17518695, 2022, 5, Downloaded from https://ietresearch.onlinelibrary.wiley.com/doi/10.1049/gtd2.12345 by Readcube (Labtiva Inc.), Wiley Online Library on [04/11/2022]. See the Terms and Conditions (https://onlinelibrary.wiley.com/terms-and-conditions) on Wiley Online Library for rules of use; OA articles are governed by the applicable Creative Commons License

where $\mathbf{x}_{inv,i} = [\delta_{inv,i}\ P_i\ Q_i\ v_{odi}\ i_{odi}\ i_{oqi}]^T$ is the state vector; $\mathbf{y}_{inv,i}$ denotes the ith inverter-interfaced DER output current; $\mathbf{D}_{inv} = [V_{busDQi}\ \omega_{com}]^T$; and ω_{com} and $\mathbf{V}_{busDQi}$ deems to be disturbances from the rest of the μG. The expressions of $\mathbf{A}_{inv,i}$, $\mathbf{B}_{inv,i}$, $\mathbf{k}_{inv,i}$, and $\mathbf{g}_{invi}$ can be written as follows:

$$\mathbf{A}_{inv,i} = \begin{bmatrix} 0 & -m_{P_i} & 0 & 0 & 0 & 0 \\ 0 & -\omega_{ci} & 0 & \omega_{ci} & \omega_{ci} & 0 \\ 0 & 0 & -\omega_{ci} & 0 & -\omega_{ci} & -\omega_{ci} \\ 0 & 0 & -k_{V_i}^{-1} n_{Q_i} & -k_{V_i}^{-1} & 0 & 0 \\ 1 & {L_{ci}}^{-1} & 0 & 0 & -R_{c_i}{L_{ci}}^{-1} & 1 \\ -1 & 0 & 0 & 0 & -1 & -R_{c_i}{L_{ci}}^{-1} \end{bmatrix}$$

$$\mathbf{B}_{inv,i} = \begin{bmatrix} \mathbf{0}_{3\times1} \\ k_{V_i}^{-1} \\ \mathbf{0}_{2\times1} \end{bmatrix},\ \mathbf{k}_{inv,i} = \begin{bmatrix} \begin{bmatrix} \mathbf{0}_{4\times2} \\ -{L_{ci}}^{-1} T_i^{-1} \end{bmatrix}_{6\times2} & \mathbf{0}_{6\times1} \\ \mathbf{0}_{6\times2} & \begin{bmatrix} -1 \\ \mathbf{0}_{5\times1} \end{bmatrix} \end{bmatrix},$$

$$\mathbf{C}_{invi} = \begin{bmatrix} \mathbf{0}_{3\times1} \\ 1 \\ \mathbf{0}_{2\times1} \end{bmatrix} \tag{9}$$

Remark 1. *(Controllability)* [35]: System (8) is controllable if for any initial state $\mathbf{x_0}$ and any final state $\mathbf{x}_f$, there exists an input sequence, which transfers $\mathbf{x_0}$ to $\mathbf{x}_f$ in a finite time interval. Otherwise, the system is uncontrollable. The system (8) is controllable if and only if Rank $[\mathbf{B}_{inv,i}\ \mathbf{A}_{inv,i}\mathbf{B}_{inv,i} \cdots \mathbf{A}_{inv,i}^{n-1}\mathbf{B}_{inv,i}] = n$. In other words, this matrix should be a full rank matrix and rows should be independent of each other. As was mentioned in [35], if matrices $\mathbf{A}_{inv,i}$ and $\mathbf{B}_{inv,i}$ are time independent, the pair ($\mathbf{A}_{inv,i}$, $\mathbf{B}_{inv,i}$) is controllable. Therefore, according to Equation (8), it can be easily concluded that this system is controllable.

2.1.3 | Network and loads model

Figure 3 shows the schematic model of the network and loads. The overall state-space model of the network including lines and loads can be written as follows:

$$\mathbf{i}_{netDQ}(t) = \mathbf{A}_{net}\mathbf{x}_{network}(t)$$
$$\mathbf{V}_{busDQ}(t) = \mathbf{C}_{bus}\mathbf{x}_{network}(t) \tag{10}$$

wherein $\mathbf{x}_{network} = [\mathbf{i}_{netDQ}\ \ \dot{\mathbf{i}}_{oDQ}\ \ \mathbf{i}_{oDQ}\ \ \omega_{com}]^T$, $\mathbf{i}_{netDQ} = [i_{lineDQ}\ \ i_{loadDQ}]^T$ is the network current, and $\mathbf{V}_{busDQ}$ represents bus voltages. The detailed expression of constant matrices of $\mathbf{A}_{net}$ and $\mathbf{C}_{bus}$ can be found in [3].

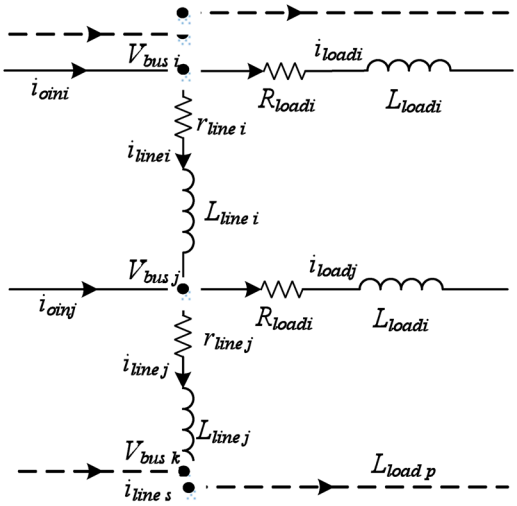

FIGURE 3 Schematic model of the network and loads

2.1.4 | Complete model of μG

By combining Equations (2)–(10), the complete dynamic model of the islanded μG can be expressed as follows:

$$\dot{\mathbf{x}}(t) = \mathbf{f}(\mathbf{x}(t)) + \mathbf{g}(\mathbf{u}(t))$$
$$\mathbf{y}(t) = \mathbf{h}(\mathbf{x}(t)) \tag{11}$$

where $\mathbf{x} = [\mathbf{x}_{syn,1}\ \ldots\ \mathbf{x}_{syn,g}\ \mathbf{x}_{inv,1}\ \ldots\ \mathbf{x}_{inv,n}\ \mathbf{i}_{line,1}\ \ldots\ \mathbf{i}_{line,s}\ \mathbf{i}_{load,1}\ \ldots\ \mathbf{i}_{load,p}]$ is μG's states; $\mathbf{u}(t)$ is the control vector of μG; and g, n, s, and p represent the number of synchronous and inverter-interfaced DERs, lines, and loads, respectively. The detailed expressions $\mathbf{f}(\mathbf{x}(t))$, $\mathbf{g}(\mathbf{u}(t))$, and $\mathbf{h}(\mathbf{x}(t))$ can be obtained by integrating Equations (2), (8), and (10). $\mathbf{y}$ represents the output variables of μG. v_{odi} and $v_{syn,i}$ are the output variables of inverter-interfaced and synchronous DERs, respectively. Note that, in order to design the proposed control method, it is necessary to obtain the discrete state-space model of a system. Toward this end, we utilized the Jacobian method as follows:

$$\mathbf{x}(k+1) = \mathbf{A}(k)\mathbf{x}(k) + \mathbf{B}(k)\mathbf{u}(k)$$
$$\mathbf{y}_{inv,i}(k) = \mathbf{C}(k)\mathbf{x}(k) \tag{12}$$

where $\mathbf{A}(k)$, $\mathbf{B}(k)$, and $\mathbf{C}(k)$ are the Jacobain terms of $\mathbf{f}(\mathbf{x}(t))$, $\mathbf{g}(\mathbf{u}(t))$, and $\mathbf{h}(\mathbf{x}(t))$, respectively, which can be calculated as $\mathbf{A}(k) = \partial\mathbf{f}(\mathbf{x})/\partial\mathbf{x}$, $\mathbf{B}(k) = \partial\mathbf{g}(\mathbf{u})/\partial\mathbf{u}$, and $\mathbf{C}(k) = \partial\mathbf{h}(\mathbf{x})/\partial\mathbf{x}$.

2.2 | DDIs and LRF conditions

Consider a discrete-time non-linear DDI as:

$$\mathbf{y}(k+1) \in \mathbf{F}(\mathbf{y}_{[k-h,k]}, \mathbf{u}(k), \mathbf{w}(k)), k \in \mathbb{Z}_+, h \geq 1 \tag{13}$$

17518695, 2022, 5, Downloaded from https://ietresearch.onlinelibrary.wiley.com/doi/10.1049/gtd2.12345 by Readcube (Labtiva Inc.), Wiley Online Library on [04/11/2022]. See the Terms and Conditions (https://onlinelibrary.wiley.com/terms-and-conditions) on Wiley Online Library for rules of use; OA articles are governed by the applicable Creative Commons License

where $\mathbf{y}_{[k-h,k]} \in \mathbb{R}^{N(h+1)}$, $\mathbf{u}(k) \in \mathbb{R}^{m}$, and $\mathbf{w}(k) \in \mathbb{R}^{c}$, represent a sequence of delayed states, inputs, and additive disturbances to model communication noises and μG uncertainties, respectively; N is the total number of DERs; m is the total number of control inputs. $\mathbf{w}(k)$ is a normal white noise vector with the intensity of η. The upper bound of time delay is denoted by $h \in \mathbb{Z}_{+}$, which is obtained later. In order to study DDI systems, it is necessary to be aware of some preliminaries and LRF conditions. The preliminaries are provided in Appendix 1.

2.3 | T-S fuzzy time-delay systems

In order to study the secondary voltage control and to design the proposed method, it is required to transform the non-linear dynamic model of μG into a linear one. The whole dynamic model of μG is achieved by fuzzy interpolation of local linear models. Based on the DDIs, the non-linear system (12) including time-varying delays and disturbances can be described by the following T-S fuzzy rule:

Plant Rule l:
IF: z_1 is F_1^l, …, and z_v is F_v^l
THEN:

$$\mathbf{y}(k+1) = \sum_{i=-h}^{0} \mathbf{A}_{i,l}\mathbf{y}(k+i) + \mathbf{B}_l\mathbf{u}(k) + \mathbf{E}_l\mathbf{w}(k) \tag{14}$$

where $\mathbf{z} := [z_1, \ldots, z_v]$ is the vector of premise variables, v is the number of premise variables, $F_1^l, \ldots, F_v^l$ fuzzy sets, $l \in \mathbb{Z}_{[1,L]}$ and L denotes the number of IF-THEN fuzzy rules, $\mathbf{A}_{i,l}$, $\mathbf{B}_l$ are discrete system matrices, $\mathbf{E}_l$ is a diagonal matrix called the disturbance matrix, and i indicates time delays and varies within $i \in [-h, 0]$. The normalized membership functions are described as follows:

$$\mu_l(z(k)) = \frac{\prod_{j=1}^{v} \mathrm{F}_j^l(z_j(k))}{\sum_{l=1}^{L}\prod_{j=1}^{v} \mathrm{F}_j^l(z_j(k))} \tag{15}$$

where $\mu_l(z(k))$ is the normalized membership function associated with the lth local system such that satisfies $\sum_{l=1}^{L}\mu_l(z(k)) = 1$ and $\mu_l(z(k)) \geq 0$. Then, the global T-S fuzzy system using Equations (15) and (16) can be written as follows:

$$\mathbf{y}(k+1) = \sum_{i=-h}^{0} \mathbf{A}_{i,\mu}\mathbf{y}(k+i) + \mathbf{B}_\mu\mathbf{u}(k) + \mathbf{E}_\mu\mathbf{w}(k) \tag{16}$$

where $\mathbf{A}_{i,\mu} := \sum_{l=1}^{L}\mu_l(z)\mathbf{A}_{i,l}$, $\mathbf{B}_\mu := \sum_{l=1}^{L}\mu_l(z)\mathbf{B}_l$, and $\mathbf{E}_\mu := \sum_{l=1}^{L}\mu_l(z)\mathbf{E}_l$. The local controller associated with each rule for the above T-S fuzzy system is given as:

Control Rule l:
IF: z_1 is F_1^l and …, z_v is F_v^l
THEN:

$$\mathbf{u}_l(k) = K_l\mathbf{y}(k) \tag{17}$$

Similar to Equation (16), the final control output can be achieved as follows:

$$\mathbf{u}(k) = K_\mu\mathbf{y}(k) \tag{18}$$

where $K_\mu = \sum_{l=1}^{L}\mu_l(z)K_l$.

3 | THE PROPOSED METHOD

3.1 | Outline

Here, the main goal is to design a novel RFMPC scheme to calculate the proper control inputs $\mathbf{u}(k)$ in Equation (11) such that output voltage amplitudes $\mathbf{v}_i$ reach to their reference values v_{ref}, i.e., $v_i \to v_{ref}$. The main contribution of the paper is that we consider three main factors which can degrade system performance. We simultaneously consider three factors including time delays, the non-linearity of microgrids, and noises, which have been overlooked in most of the previous works. Another contribution is that we examined the computation burden. The previously proposed methods focused only on improving dynamical response and neglected computation effort. In this paper, we propose a method in order to reduce the computation effort by separating the original objective function into offline and online stages. The proposed method includes two stages: offline and online. In the offline stage, a sequence of control constraint sets is obtained and then we attempt to find the optimal one, which is not analysed in the existing methods. Afterwards, in the online stage, an optimization problem is solved by considering the optimal region.

3.2 | Control objective

Consider the following prediction model for the T-S fuzzy system (14) as follows:

$$\mathbf{y}(k+s+1|k) = \sum_{i=-h}^{0} \mathbf{A}_{i,\mu}\mathbf{y}(k+s+i|k) + \mathbf{B}_\mu\mathbf{u}(k+s|k) + \mathbf{E}_\mu\mathbf{w}(k+s|k) \tag{19}$$

At the time slot k, a finite horizon objective function is defined as follows:

$$J(k) = \sum_{s=0}^{H_p-1} \ell(\mathbf{y}(k+s|k)) + \mathrm{V}_T(\mathbf{y}(k+H_P|k)) \tag{20}$$

where $\ell(k+s|k)$ and $\mathrm{V}_T(\mathbf{y}(k+H_P|k)$ are stage and terminal costs, respectively; H_p is the prediction horizon; and $s \in \mathbb{Z}_{[0,H_p-1]}$ is the sth predicted time step. Stage cost is defined as:

$$\ell(k+s|k) = (\mathbf{y}(k+s|k) - \mathbf{y}_r(k+s|k))^T\,\mathrm{Q}(\mathbf{y}(k+s|k) - \mathbf{y}_r(k+s|k)) + \mathbf{u}^T(k+s|k)\mathbf{R}\mathbf{u}k+s|k) - \psi\mathbf{w}^T(k+s|k)\mathbf{w}(k+s|k) \tag{21}$$

17518695, 2022, 5, Downloaded from https://ietresearch.onlinelibrary.wiley.com/doi/10.1049/gtd2.12345 by Readcube (Labtiva Inc.), Wiley Online Library on [04/11/2022]. See the Terms and Conditions (https://onlinelibrary.wiley.com/terms-and-conditions) on Wiley Online Library for rules of use; OA articles are governed by the applicable Creative Commons License

where $\mathbf{Q}, \mathbf{R} \succ 0$ are weighted matrices, and ψ is a positive scalar. The terminal cost function ensures that the output variables reach their reference values at the end of the prediction horizon and can be defined as follows:

$$V_T(\mathbf{y}(k+H_P|k)) = \sum_{l=1}^{L} \mu(\mathbf{y})(\mathbf{y}-\mathbf{y}_r)^T \mathbf{P}_l (\mathbf{y}-\mathbf{y}_r) \tag{22}$$

where $\mathbf{P}_l \succ 0$ is a weighted matrix.

Since the objective function (20) includes the information of disturbances, it cannot be optimized directly; thus, a min-max method is exploited so that the worst-case objective function is minimized. In addition, it is mandatory that the DERs' output voltages enter a terminal constraint set Ω_t at the end of the prediction horizon, i.e., $\mathbf{y}(k+H_P|k) \in \Omega_t$. Thus, the online optimization problem can be given at each time instant k as:

$$\min_{\mathbf{u}(k+s|k)} \max_{\mathbf{w}(k+s|k)} J(k) \tag{23}$$

subject to:

$$\mathbf{w}(k+l|k) \in \mathbb{W} \tag{24a}$$

$$\mathbf{y}(k+H_P|k) \in \Omega_t \tag{24b}$$

$$\mathbf{u}(k) \in \mathbb{U} \tag{24c}$$

where Ω_t is the terminal constraint; $\mathbb{W}$ and $\mathbb{U}$ are two compact sets including the origin point such that satisfy:

$$\begin{aligned} \mathbf{u} \in \mathbb{U} &\stackrel{\Delta}{=} \left\{\mathbf{u} \middle| |\mathbf{u}_t| \le \mathbf{u}_{t,max}\right\} \\ \mathbf{w} \in \mathbb{W} &\stackrel{\Delta}{=} \left\{\mathbf{w} \middle| \mathbf{w}^T\mathbf{w} \le \eta^2\right\} \end{aligned} \tag{25}$$

where η is a known positive constant, $\mathbf{u}_{t,max}$ is the maximum value of tth element of the control input vector, $t \in \mathbb{Z}_{[1,m]}$. It is obvious that each distributed generator has a limited capacity to regulate its output variable. For example, a synchronous generator cannot supply any desired load demand because of its limited shaft torque, which prevents it from providing the required torque. Otherwise, it will be damaged. Moreover, inverter-interfaced DERs cannot increase their outputs to any wanted value since their converters have limited capacity, and by increasing from their limits, their converters will be damaged. Therefore, control signals limitations should be considered while designing a control method. For this reason, the maximum control inputs values have been considered in Equation (25) and in the following procedure. Also, according to Equation (25), any type of disturbances that is bounded can be used in the designing process. However, in this paper, for the sake of simplicity and also because of its practical point of view, normal white Gaussian noise is incorporated in this paper.

3.3 | Offline stage

In this subsection, the goal is to design the offline stage of the proposed method. Toward this end, first, a convergence region for output variables is defined, called the terminal constraint set (see Appendix 2), and then, using that, a sequence of constraint sets will be obtained. Finally, an optimal convergence region is calculated.

In the following, we develop the inequality (53), presented in Appendix 2, to acquire a sequence of terminal constraint sets related to a sequence of control laws. To do so, define a robust constraint set $\Omega_e(\Omega_e \supseteq \Omega_t)$ such that all system states, including the current and delayed states, enter Ω_e, that is, $\mathbf{y}(k+i)_{\forall i \in \mathbb{Z}_{[-b,0]}} \in \Omega_e$. Ω_e is called the optimal convergence constraint set. According to Definition 1, a control law π_e is given such that ensures the system states in the next instant enter Ω_t, that is, $\mathbf{y}^+ \in \Omega_t$. Obviously, since $\Omega_t \subseteq \Omega_e$, it is guaranteed that Ω_e is positive invariance. After computation of Ω_e and the related control law π_e, in a similar way, a sequence of robust constraint sets $\{\Omega_0, \Omega_1, \cdots, \Omega_e, \cdots, \Omega_{\tilde{N}}\}$ corresponding to a sequence of control laws $\{\pi_0, \pi_1, \cdots, \pi_e, \cdots, \pi_{\tilde{N}}\}$ can be obtained, in which Ω_0 and π_0 represent the terminal set Ω_t and related control law π_t, respectively.

First of all, suppose that there exists two successive robust constraint sets Ω_{e-1} and Ω_e such that $\Omega_{e-1} \subseteq \Omega_e$. From the aforementioned design principle, if it is assumed that $\mathbf{y}(k+i)_{\forall i \in \mathbb{Z}_{[-b,0]}} \in \Omega_e$, then $\mathbf{y}^+ \in \Omega_{e-1}$ can be satisfied by the following inequality:

$$\begin{aligned} &\left(\mathbf{y}^+ - \mathbf{y}_r^+\right)^T \mathbf{X}_{e-1}^{-1} \left(\mathbf{y}^+ - \mathbf{y}_r^+\right) - (1-\lambda) \\ &\max_{i \in \mathbb{Z}_{[-b,0]}} \left\{(\mathbf{y}(k+i) - \mathbf{y}_r(k+i))^T \mathrm{X}_e^{-1} (\mathbf{y}(k+i) - \mathbf{y}_r(k+i))\right\} \\ &- \frac{\lambda}{\eta^2} \mathbf{w}^T(k)\, \mathbf{w} \end{aligned} \tag{26}$$

where $\mathbf{X}_e$ and $\mathbf{X}_{e-1}$ are positive definite matrices related to constraint sets $\Omega_e = \{\mathbf{y} | (\mathbf{y}-\mathbf{y}_r)^T \mathbf{X}_e^{-1} (\mathbf{y}-\mathbf{y}_r) \le 1\}$ and $\Omega_{e-1} = \{\mathbf{y} | (\mathbf{y}^+ - \mathbf{y}_r^+)^T \mathbf{X}_{e-1}^{-1} (\mathbf{y}^+ - \mathbf{y}_r^+) \le 1\}$, respectively. Similar to Equation (52) in Appendix 2, if $\max_{i \in \mathbb{Z}_{[-b,0]}} \{(\mathbf{y}(k+i) - \mathbf{y}_r(k+i))^T \mathbf{X}_e^{-1} (\mathbf{y}(k+i) - \mathbf{y}_r(k+i))\} \le 1$, then Equation (26) guarantees $(\mathbf{y}^+ - \mathbf{y}_r^+)^T \mathbf{X}_{e-1}^{-1} (\mathbf{y}^+ - \mathbf{y}_r^+) \le 1$.

Second, the optimization control can be described as:

$$\begin{aligned} &\left(\mathbf{y}^+ - \mathbf{y}_r^+\right)^T \mathbf{P}_e \left(\mathbf{y}^+ - \mathbf{y}_r^+\right) \\ &- \max_{i \in \mathbb{Z}_{[-b,0]}} \left\{(\mathbf{y}(k+i) - \mathbf{y}_r(k+i))^T \mathbf{P}_e (\mathbf{y}(k+i) - \mathbf{y}_r(k+i))\right\} \\ &\leftarrow (\mathbf{y}(k) - \mathbf{y}_r(k))^T \mathbf{Q} (\mathbf{y}(k) - \mathbf{y}_r(k)) - \mathbf{u}^T(k) \mathbf{R} \mathbf{u}(k) \end{aligned} \tag{27}$$

17518695, 2022, 5, Downloaded from https://ietresearch.onlinelibrary.wiley.com/doi/10.1049/gtd2.12345 by Readcube (Labtiva Inc.), Wiley Online Library on [04/11/2022]. See the Terms and Conditions (https://onlinelibrary.wiley.com/terms-and-conditions) on Wiley Online Library for rules of use; OA articles are governed by the applicable Creative Commons License

Now the two aforementioned requirements, inspired by our previous research work [33], will be provided in the form of matrix inequalities. Toward this end, Theorem 2 in Appendix 2 is developed to obtain a sequence of robust constraint sets.

Theorem 1. *Suppose Ω_{e-1} is an already-known constraint set. The set Ω_e is an RPI set for the T-S fuzzy system (16) with respect to the corresponding feedback control law π_e, if there exists a positive definite matrix $\mathbf{X}_e$, general matrices $\mathbf{Y}_a$, $\mathbf{Y}_b$, $\mathbf{Y}_l$, $\mathbf{Z}$, and two positive scalars $\xi_e, \lambda \in \mathbb{R}_{(0,1)}$, such that the following matrix inequalities are feasible:*

$$\begin{bmatrix} \boldsymbol{\phi}_0 & \mathbf{0} & \cdots & \mathbf{0} & \mathbf{0} & \boldsymbol{\Gamma}_0^T \\ \mathbf{0} & \boldsymbol{\phi}_1 & \cdots & \cdots & \cdots & \boldsymbol{\Gamma}_1^T \\ \vdots & \vdots & \ddots & \vdots & \vdots & \vdots \\ \mathbf{0} & \mathbf{0} & \cdots & \boldsymbol{\phi}_b & \mathbf{0} & \boldsymbol{\Gamma}_b^T \\ \mathbf{0} & \mathbf{0} & \cdots & \mathbf{0} & -\frac{\lambda}{\eta^2} I & (\mathbf{E}_a)^T \\ \boldsymbol{\Gamma}_0 & \boldsymbol{\Gamma}_1 & \cdots & \boldsymbol{\Gamma}_b & \mathbf{E}_a & -\mathbf{X}_{e-1} \end{bmatrix} \leq 0 \tag{28a}$$

$$\begin{bmatrix} \boldsymbol{\Xi}_0 & 0 & \cdots & \mathbf{0} & \boldsymbol{\Gamma}_0^T & (\mathbf{Q}\mathbf{X}_e)^T & (\mathbf{R}\mathbf{Y}_b)^T \\ \mathbf{0} & \boldsymbol{\Xi}_1 & \cdots & \cdots & \boldsymbol{\Gamma}_1^T & \mathbf{0} & \mathbf{0} \\ \vdots & \vdots & \ddots & \vdots & \vdots & \vdots & \vdots \\ \mathbf{0} & \mathbf{0} & \cdots & \boldsymbol{\Xi}_b & \boldsymbol{\Gamma}_b^T & \mathbf{0} & \mathbf{0} \\ \boldsymbol{\Gamma}_0 & \boldsymbol{\Gamma}_1 & \cdots & \boldsymbol{\Gamma}_b & -\mathbf{X}_e & \mathbf{0} & \mathbf{0} \\ \mathbf{Q}\mathbf{X}_e & \mathbf{0} & \cdots & \mathbf{0} & \mathbf{0} & -\xi_e \mathbf{Q} & \mathbf{0} \\ \mathbf{R}\mathbf{Y}_b & \mathbf{0} & \cdots & \mathbf{0} & \mathbf{0} & \mathbf{0} & -\xi_e \mathbf{R} \end{bmatrix} < 0 \tag{28b}$$

$$\begin{bmatrix} \mathbf{Z} & \mathbf{Y}_b \\ \mathbf{Y}_b^T & \mathbf{X}_e \end{bmatrix} \geq 0, \quad Z_{tt} \leq \mathrm{u}_{t,max}^2, \quad t \in \mathbb{Z}_{[0,m]} \tag{28c}$$

where $\mathbf{0}$ and $\boldsymbol{I}$ are zero and identity matrices; $a, b \in \mathbb{Z}_{[1,L]}$, $\mathbf{Z}_{tt}$ is the tth diagonal element of matrix $\mathbf{Z}$; $\boldsymbol{\phi}_{-i} = \gamma_i(\lambda - 1)\mathbf{X}_e$, $\boldsymbol{\Xi}_{-i} = -\gamma_i \mathbf{X}_e$, $i \in \mathbb{Z}_{[-b,0]}$, γ_i are positive numbers such that $\sum_{i=-b}^{0} \gamma_i = 1$; $\boldsymbol{\Gamma}_0 = \mathbf{A}_{0,a}\mathbf{X}_e + \mathbf{B}_a \mathbf{Y}_b$, $\boldsymbol{\Gamma}_{-j} = \mathbf{A}_{j,a}\mathbf{X}_e$, $j \in \mathbb{Z}_{[-b,-1]}$; $\mathbf{P}_e = \xi_e \mathbf{X}_e^{-1}$; $\pi_e = K_\mu \mathbf{y}$, with $K_\mu = \sum_{l=1}^{L} \mu_l K_l$ and $K_l = \mathbf{Y}_l \mathrm{X}_e^{-1}$. Note that, in this paper, we assume that the output variable at each time instant is related to the control input at that time instant. In other words, we consider delay on output variables, not on control input vectors. For this reason, matrix $\mathbf{B}_a$ is considered only at time instant 0.

Proof. The proof of this theorem is so similar to Theorem 2 in Appendix 2.

Remark 2. Coefficients γ_i are called the confidence levels taking into account the effect of communication latency such that $\sum_{i=-b}^{0} \gamma_i = 1$.

3.4 | Online stage

Consider the following prediction model without noises and uncertainties:

$$\mathbf{y}(k+s+1|k) = \sum_{i=-b}^{0} \mathbf{A}_{i,\mu} \mathbf{y}(k+s+i|k) + \mathbf{B}_\mu \mathbf{u}(k+s|k) \tag{29}$$

The function $J_1(k)$ is defined as follows:

$$\begin{aligned} J_1(k) :=\ & (\mathbf{y}(k) - \mathbf{y}_r(k))^T \mathbf{Q} (\mathbf{y}(k) - \mathbf{y}_r(k)) + \mathbf{u}^T \mathbf{R} \mathbf{u}(k) \\ & + (\mathbf{y}(k+1|k) - \mathbf{y}_r(k+1|k))^T \mathbf{P}_{e-1} (\mathbf{y}(k+1|k) \\ & - \mathbf{y}_r(k+1|k)) \end{aligned} \tag{30}$$

Optimization and minimization of $J_1(k)$ is conducted online. Now, we are ready to present the optimization problem of RFMPC. Based on the derived sequence of terminal constraint sets in Equation (28), at each time instant k, the optimization problem can be summarized as:

$$\min_{\mathbf{u}(k)} \psi \tag{31}$$

subject to:

$$J_1(k) \leq \psi \tag{32a}$$

$$\mathbf{y}(k+1|k) \in \Omega_{e-1} \tag{32b}$$

$$\mathbf{u}(k) \in \mathbb{U} \tag{32c}$$

wherein $\Omega_{e-1} = \{\mathbf{y} | (\mathbf{y} - \mathbf{y}_r)^T \mathbf{P}_{e-1} (\mathbf{y} - \mathbf{y}_r) \leq \xi_{e-1}\}$. In what follows, it is attempted to represent the constraints of the optimization problem (31) in the form of some LMIs. To this aim, by substituting $\mathbf{y}(k+1) = \sum_{i=-b}^{0} \mathbf{A}_{i,\mu} \mathbf{y}(k+i) + \mathbf{B}_\mu \mathbf{u}(k)$ into Equation (32a), one has:

$$\begin{aligned} & (\mathbf{y}(k) - \mathbf{y}_r(k))^T \mathbf{Q} (\mathbf{y}(k) - \mathbf{y}_r(k)) + \mathbf{u}^T(k) \mathbf{R} \mathbf{u}(k) \\ & + [\mathbf{A}_\mu \mathbf{y}(k) + \mathbf{B}_\mu \mathbf{u}(k)]^T \mathbf{P}_{e-1}^{-1} [\mathbf{A}_\mu \mathbf{y}(k) + \mathbf{B}_\mu \mathbf{u}(k)] \leq \psi \end{aligned} \tag{33}$$

The above inequality can be developed equivalently to:

$$\begin{bmatrix} -\psi + (\mathbf{y}(k) - \mathbf{y}_r(k))^T \mathbf{Q} (\mathbf{y}(k) - \mathbf{y}_r(k)) & \varsigma^T & \mathbf{u}^T(k) \\ \varsigma & -\mathbf{P}_{e-1}^{-1} & \mathbf{0} \\ \mathbf{u}(k) & \mathbf{0} & -\mathbf{R}^{-1} \end{bmatrix} \leq 0 \tag{34}$$

where $\varsigma = \sum_{i=-b}^{0} \mathbf{A}_{i,\mu} \mathbf{y}(k+i) + \mathbf{B}_\mu \mathbf{u}(k)$.

17518695, 2022, 5, Downloaded from https://ietresearch.onlinelibrary.wiley.com/doi/10.1049/gtd2.12345 by Readcube (Labtiva Inc.), Wiley Online Library on [04/11/2022]. See the Terms and Conditions (https://onlinelibrary.wiley.com/terms-and-conditions) on Wiley Online Library for rules of use; OA articles are governed by the applicable Creative Commons License

Consider constraint (32b), which equivalently can be written without considering disturbances as:

$$(\mathbf{y}(k+1)-\mathbf{y}_r(k+1))^T\mathbf{P}_{e-1}(\mathbf{y}(k+1)-\mathbf{y}_r(k+1)) \le \xi_{e-1} \tag{35}$$

The above inequality is developed to consider noises and disturbances. By taking into account the disturbances $\mathbf{w}^T(k)\mathbf{w}(k) \le \eta^2$, inequality (35) holds if and only if:

$$(\mathbf{y}(k+1)-\mathbf{y}_r(k+1))^T\mathbf{P}_{e-1}(\mathbf{y}(k+1)-\mathbf{y}_r(k+1))-\xi_{e-1} -\lambda(\mathbf{w}^T(k)\mathbf{w}(k)-\eta^2) \le 0 \tag{36}$$

where $\lambda > 0$ is a scalar. By considering that $\mathbf{y}(k+1) = \sum_{i=-h}^{0}\mathbf{A}_{i,\mu}\mathbf{y}(k+i)+\mathbf{B}_\mu\mathbf{u}(k)+\mathbf{E}_\mu\mathbf{w}(k)$, the inequality (36) can be written as follows:

$$\begin{bmatrix}1 & \mathbf{w}^T(k)\end{bmatrix}\begin{bmatrix}\mathbf{\Theta}_{11} & \mathbf{\Theta}_{12}\\ \mathbf{\Theta}_{21} & \mathbf{\Theta}_{22}\end{bmatrix}\begin{bmatrix}1\\ \mathbf{w}(k)\end{bmatrix} \le 0 \tag{37}$$

where $\mathbf{\Theta}_{11} = [\sum_{i=-h}^{0}\mathbf{A}_{i,\mu}\mathbf{y}(k+i)+\mathbf{B}_\mu\mathbf{u}(k)]^T\mathbf{P}_{e-1}[\sum_{i=-h}^{0}\mathbf{A}_{i,\mu}\mathbf{y}(k+i)+\mathbf{B}_\mu\mathbf{u}(k)]-\xi_{e-1}+\lambda\eta^2$, $\mathbf{\Theta}_{12} = [\mathbf{A}_\mu\mathbf{y}(k)+\mathbf{B}_\mu\mathbf{u}(k)]^T\mathbf{P}_{e-1}\mathbf{E}_\mu$, $\mathbf{\Theta}_{22} = \mathbf{E}_\mu^T\mathbf{P}_{e-1}\mathbf{E}_\mu-\lambda$, $\mathbf{\Theta}_{21} = \mathbf{\Theta}_{12}^T$. The inequality (37) holds if:

$$\begin{bmatrix}\mathbf{\Theta}_{11} & \mathbf{\Theta}_{12}\\ \mathbf{\Theta}_{21} & \mathbf{\Theta}_{22}\end{bmatrix} \le 0 \tag{38}$$

The above equation can be written as:

$$\begin{bmatrix}-\xi_{e-1}+\lambda\eta^2 & 0\\ 0 & -\lambda\end{bmatrix}+\begin{bmatrix}\varsigma^T\mathbf{P}_{e-1}\varsigma & \varsigma^T\mathbf{P}_{e-1}\mathbf{E}_\mu\\ (\varsigma^T\mathbf{P}_{e-1}\mathbf{E}_\mu)^T & \mathbf{E}_\mu^T\mathbf{P}_{e-1}\mathbf{E}_\mu\end{bmatrix} \le 0 \tag{39}$$

where $\varsigma = \sum_{i=-h}^{0}\mathbf{A}_{i,\mu}\mathbf{y}(k+i)+\mathbf{B}_\mu\mathbf{u}(k)$. This equation can be shown as follows:

$$\begin{bmatrix}-\xi_{e-1}+\lambda\eta^2 & 0\\ 0 & -\lambda\end{bmatrix}+\begin{bmatrix}\varsigma^T\\ \mathbf{E}_\mu\end{bmatrix}\mathbf{P}_{e-1}[\varsigma^T \quad \mathbf{E}_\mu] \le 0 \tag{40}$$

By applying the Schur complement, the above inequality can be equivalently written as:

$$\begin{bmatrix}-\xi_{e-1}+\lambda\eta^2 & 0 & \varsigma^T\\ 0 & -\lambda & \mathbf{E}_\mu^T\\ \varsigma & \mathbf{E}_\mu & -\mathbf{P}_{e-1}^{-1}\end{bmatrix} \le 0 \tag{41}$$

The input constraint (32c) can be guaranteed by:

$$\begin{bmatrix}\mathbf{Z} & \mathbf{u}(k)\\ \mathbf{u}^T(k) & \mathbf{I}\end{bmatrix} \ge 0 \tag{42}$$

ALGORITHM 1 RFMPC for the secondary voltage control

Offline stage computation:

1: Compute the terminal constraint set Ω_0 and the corresponding feedback control law π_0 using the method described in Theorem 2 in Appendix 2.

2: Based on the obtained terminal constraint set, compute a sequence of terminal constraint sets $\{\Omega_0,\Omega_1,\cdots,\Omega_{\bar{N}}\}$ and the corresponding control laws $\{\pi_0,\pi_1,\cdots,\pi_e,\cdots,\pi_{\bar{N}}\}$ using the method described in Theorem 1.

Online stage computation:

3: Set $k = 0$.

4: Obtain the μG outputs $\mathbf{y}(k)$ at time k. If $\mathbf{y}(k+i)_{\forall i\in\mathbb{Z}_{[-h,0]}} \in \Omega_{\bar{N}}$ feed the μG with control laws obtained in Step 2; Else, find the index e such that $\mathbf{y}(k+i)_{\forall i\in\mathbb{Z}_{[-h,0]}} \in \Omega_e\backslash\Omega_{e-1}$, if $\Omega_e = \Omega_0$, then the corresponding control law for Ω_0 is fed to μG for all k. Otherwise, go to Step 5.

5: Solve the constrained optimization problem (43), obtain the control input, and feed it to the μG.

6: k: = k+1 and go to Step 4.

with $\mathbf{Z}_{tt} \le \mathbf{u}_{t,max}^2, t \in \mathbb{Z}_{[0,m]}$. The constrained online optimization problem (31) considering developed matrix inequalities is briefly given as follows:

$$\min_{\mathbf{u}(k),\psi,\lambda,\mathbf{Z}} \psi, \tag{43}$$

subject to Equations (34), (41), and (42)

3.5 | Control algorithm

The proposed RFMPC control algorithm is summarized in Algorithm 1.

Remark 3. The inequality (28) is a bilinear matrix inequality (BMI) due to the presence of the bilinear variable λ. Therefore, the PENLAB solver is utilized to solve the BMI problems. Doing so, the optimal value of λ is computed in the offline stage, and the online stage is reduced to solving an LMI problem, as a result of which computation burden will be reduced to a great extent.

Remark 4. In Theorem 1, in order to find $\mathbf{X}_e$, we suppose that Ω_{e-1} is an already-known constraint set, which means that $\mathbf{X}_{e-1}$ is an already-known matrix. According to Algorithm 1, first, Ω_t should be obtained. Toward this end, $\mathbf{X}_t$ could be an arbitrary positive definite matrix. Without loss of generality, in this paper, we consider $\mathbf{X}_t$ as an identity matrix, which is positive definite. After obtaining Ω_t, we try to find index e such that $\mathbf{y}(k+i)_{\forall i\in\mathbb{Z}_{[-h,0]}} \in \Omega_e\backslash\Omega_{e-1}$.

Remark 5. (bump-less operation): Bump-less operation means that the output variable does not change abruptly while switching between controllers. In other words, the objective of bump-less operation is to provide control logic that enables a smooth transition from one controller to another one. To prove the bump-less operation of the proposed

17518695, 2022, 5, Downloaded from https://ietresearch.onlinelibrary.wiley.com/doi/10.1049/gtd2.12345 by Readcube (Labtiva Inc.), Wiley Online Library on [04/11/2022]. See the Terms and Conditions (https://onlinelibrary.wiley.com/terms-and-conditions) on Wiley Online Library for rules of use; OA articles are governed by the applicable Creative Commons License

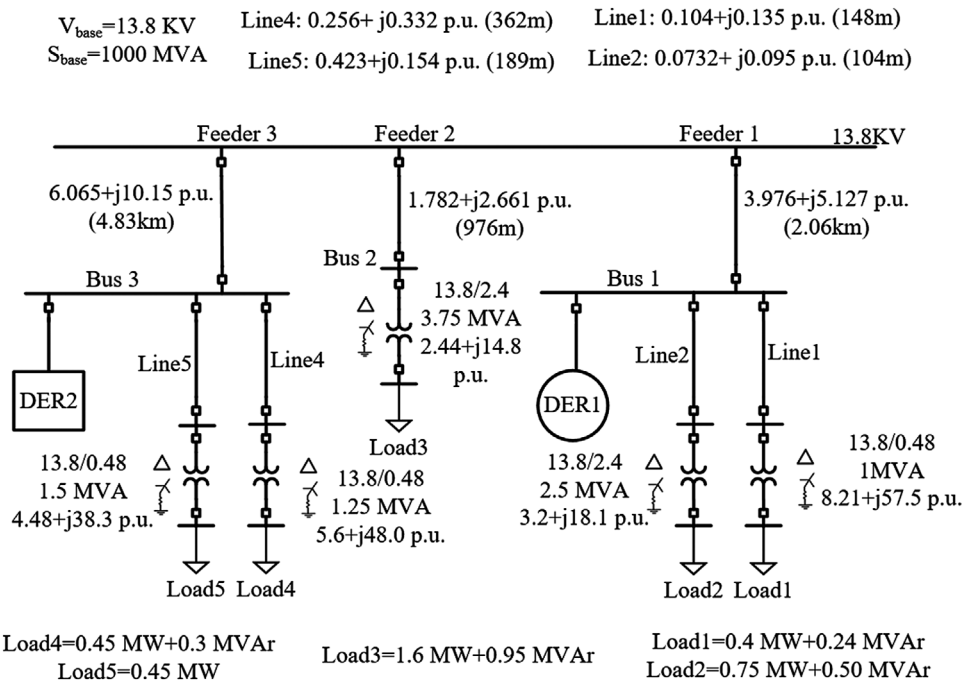

FIGURE 4 Single-line diagram of the test system

algorithm, consider the Lyapunov function $\bar{V}(\mathbf{y}(k)) = \max_{i\in\mathbb{Z}_{[-h,0]}} \{V(\mathbf{y}(k+i) - \mathbf{y}_r(k+i))\}$. According to Equation (B3b), presented in Appendix 2, one has:

$$\begin{aligned} &V(\mathbf{y}^+ - \mathbf{y}_r^+) - \bar{V}(\mathbf{y}(k) - \mathbf{y}_r(k)) \leq \\ &-(\mathbf{y}(k) - \mathbf{y}_r(k))^T \mathbf{Q}(\mathbf{y}(k) - \mathbf{y}_r(k)) - \mathbf{u}^T(k)\mathbf{R}\mathbf{u}(k) \\ &+\psi \mathbf{w}^T(k+s|k)\mathbf{w}(k+s|k) \end{aligned} \tag{44}$$

where $V(\mathbf{y}^+ - \mathbf{y}_r^+) = (\mathbf{y}^+ - \mathbf{y}_r^+)^T \mathbf{Q}(\mathbf{y}^+ - \mathbf{y}_r^+)$. Therefore, we can obtain:

$$\begin{aligned} &V\left(\mathbf{y}^+ - \mathbf{y}_r^+\right) - \bar{V}(\mathbf{y}(k) - \mathbf{y}_r(k)) \leq \\ &-(\mathbf{y}(k) - \mathbf{y}_r(k))^T \mathbf{Q}(\mathbf{y}(k) - \mathbf{y}_r(k)) \\ &+\psi \mathbf{w}^T(k+s|k)\,\mathbf{w}(k+s|k) \end{aligned} \tag{45}$$

Owing to the optimality of Equation (43) at time $k+1$, it holds:

$$V\left(\mathbf{y}^+ - \mathbf{y}_r^+\right) \leq \bar{V}(\mathbf{y}(k) - \mathbf{y}_r(k)) \tag{46}$$

Therefore, the output variable of μG cannot change abruptly, meaning the bump-less operation of our proposed method.

4 | SIMULATION RESULTS

To validate the effectiveness and robustness of the proposed RFMPC control scheme, an autonomous μG test system, shown in Figure 4, is developed in MATLAB/Simulink software, and all matrix inequalities are solved by the YALMIP toolbox. The specifications of DERs can be found in [36] and other parameters are shown in Figure 4. The μG consists of two DERs: A small-scale single-mass synchronous generator DER1 with the total capacity of 5 MVA located on feeder $F1$; and an inverter-interfaced DER2 with the total capacity of 2.5 MVA located on feeder $F3$. The reference value of voltage magnitudes is set to $\mathbf{y}_r(k) = \mathbf{1}$. Moreover, the prediction horizon is selected as $H_p = 10$. Another important issue in secondary control of μG is the selection of sampling rates. Sampling speeds of the communication systems can heavily affect the efficiency of μG. To this end, first of all, note that the sampling rate is chosen such that the primary control response is completely done. Otherwise, both primary and secondary controllers may interfere. In addition, from the viewpoint of economic issues, operators utilize the systems that keep sampling rates as low as possible in order to reduce their cost; as a result, they can carry out control methods on slower computers, not high rate and expensive computers. High rate sampling (e.g. too short sampling period) will overload unnecessarily the processor. On the other hand, by selecting too long sampling periods, the dynamics of μG will be lost and missed. If the sampling rate is too low, the control systems may even become unstable. In conclusion, selecting the sampling period is an engineering decision that has to balance between two opposite requirements: Cost and accuracy. Considering the above explanations, the period of sampling is considered 100 ms, which is a reasonable choice.

The maximum control inputs are considered as: $\tau_{m,i}^{\max} = 10$, $v_{fd,i}^{\max} = 10$, and $u_{inv,i}^{\max} = 5$. The disturbance matrix is selected as

17518695, 2022, 5, Downloaded from https://ietresearch.onlinelibrary.wiley.com/doi/10.1049/gtd2.12345 by Readcube (Labtiva Inc.), Wiley Online Library on [04/11/2022]. See the Terms and Conditions (https://onlinelibrary.wiley.com/terms-and-conditions) on Wiley Online Library for rules of use; OA articles are governed by the applicable Creative Commons License

TABLE 1 Fuzzy model parameters of μG

	Inserted Values		Membership Functions	
Non-linear Items	**Min**	**Max**	**Min**	**Max**
$z_1 = \sin\delta_{syn}$	0.38	0.89	$F_{11} = \frac{0.89 - \sin\delta_{syn}}{0.51}$	$F_{21} = \frac{\sin\delta_{syn} - 0.38}{0.51}$
$z_2 = \cos\delta_{syn}$	0.45	0.92	$F_{12} = \frac{0.92 - \cos\delta_{syn}}{0.47}$	$F_{22} = \frac{\sin\delta_{syn} - 0.45}{0.47}$
$z_3 = \frac{\sin\delta_{syn}}{\delta_{syn}}$	0.81	0.97	$F_{13} = \frac{0.97 - \frac{\sin\delta_{syn}}{\delta_{syn}}}{0.16}$	$F_{23} = \frac{\frac{\sin\delta_{syn}}{\delta_{syn}} - 0.81}{0.16}$
$z_4 = \frac{\cos\delta_{syn}}{\delta_{syn}}$	0.41	2.30	$F_{14} = \frac{2.30 - \frac{\cos\delta_{syn}}{\delta_{syn}}}{1.89}$	$F_{24} = \frac{\frac{\cos\delta_{syn}}{\delta_{syn}} - 0.41}{1.89}$
$z_5 = \sin\delta_{inv}$	0.38	0.89	$F_{15} = \frac{0.89 - \sin\delta_{inv}}{0.51}$	$F_{25} = \frac{\sin\delta_{inv} - 0.38}{0.51}$
$z_6 = cos\delta_{inv}$	0.45	0.92	$F_{16} = \frac{0.92 - \cos\delta_{inv}}{0.47}$	$F_{26} = \frac{\cos\delta_{inv} - 0.45}{0.47}$

$\mathbf{E}_l = \text{diag}\{0.1, 0.1, 0.1\}$. The intensity of white Gaussian noise is considered as $\eta = 0.2$. Additionally, in order to verify the robustness of the proposed RFMPC scheme, the μG are parameters, and inkling line impedances and load values are perturbed intentionally with 20% additive uncertainties. The acceptable range for output voltages is considered as $1 \pm 3\%$ p.u. Without loss of generality, the weighted matrices $\mathbf{Q}$ and $\mathbf{R}$ for the objective function (21) are selected as identity matrices. For the implementation of the T-S fuzzy model, various simulations have been performed in the MATLAB software, and it is observed that the DERs' angles vary within $[\delta_{\min}, \delta_{\max}] = [23^\circ, 63^\circ]$. According to the large-signal dynamic model of DERs presented in Section 2, the μG non-linear model has four non-linear terms, including $\frac{\cos\delta}{\delta}, \frac{\sin\delta}{\delta}$,cos δ, and sin δ, for synchronous generator DER1 and two non-linear terms, including cos δ*and* sin δ, for inverter-interfaced DER2. Consequently, there are six premise variables, that is, $v = 6$, z_j for $j = 1, \ldots, v$; and then, we get $r = 2^v$ ($2^{(4+2)} = 2^6 = 64$) IF-THEN fuzzy rules. Based on the sector non-linearity approach, the membership functions are defined so that to satisfy the following two conditions:

$$\begin{aligned} \mathrm{F}_{1j}(z_j) + \mathrm{F}_{2j}(z_j) &= 1 \\ z_j &= \mathrm{F}_{1j}(z_j)(z_{j,min}) + \mathrm{F}_{2j}(z_j)(z_{j,\max}) \end{aligned} \tag{47}$$

By solving the above equations, we have:

$$\mathrm{F}_{1j}(z_j) = \frac{z_{j,\max} - z_j}{z_{j,\max} - z_{j,\min}}, \mathrm{F}_{2j}(z_j) = 1 - \mathrm{F}_{1j}(z_j) \tag{48}$$

The membership functions $\mathrm{F}_{1j}(z_j)$ and $\mathrm{F}_{2j}(z_j)$ are called as "Min" and "Max", respectively. The maximum and minimum values of the premise variables and associated membership functions are described in Table 1. Accordingly, the fuzzy rules will be defined as follows:

Rule 1 : IF z_1, z_2, z_3, z_4, z_5, and z_6 is $z_{1,min}, z_{2,min}, z_{3,min}, z_{4,min}, z_{5,min}, z_{6,min}$

THEN

$$\mathbf{y}(k+1) = \sum_{i=-h}^{0} \mathbf{A}_{i,1}\mathbf{y}(k+i) + \mathbf{B}_1\mathbf{u}(k) + \mathbf{E}_1\mathbf{w}(k)$$

Rule 2: IF z_1, z_2, z_3, z_4, z_5, and z_6 is $z_{1,min}, z_{2,min}, z_{3,min}, z_{4,min}, z_{5,min}, z_{6,max}$

THEN

$$\mathbf{y}(k+1) = \sum_{i=-h}^{0} \mathbf{A}_{i,2}\mathbf{y}(k+i) + \mathbf{B}_2\mathrm{u}(k) + \mathbf{E}_2\mathbf{w}(k)$$

$$\vdots$$

Rule 64: IF z_1, z_2, z_3, z_4, z_5, and z_6 is $z_{1,max}, z_{2,max}, z_{3,max}, z_{4,max}, z_{5,max}, z_{6,max}$

THEN

$$\mathbf{y}(k+1) = \sum_{i=-h}^{0} \mathbf{A}_{i,64}\mathbf{y}(k+i) + \mathbf{B}_{64}\mathbf{u}(k) + \mathbf{E}_{64}\mathbf{w}(k)$$

For example, in order to find the matrix A_1, non-linear terms $\sin\delta_{syn}$, $\cos\delta_{syn}$, $\frac{\sin\delta_{syn}}{\delta_{syn}}$, and $\frac{\cos\delta_{syn}}{\delta_{syn}}$ in the synchronous DER are replaced by 0.38, 0.45, 0.81, and 0.41, and non-linear terms $\sin\delta_{inv}$ and $\cos\delta_{inv}$ in the inverter-interfaced DER are replaced by 0.38 and 0.45, respectively.

4.1 | Controller performance

In this case study, a number of simulations are carried out to verify the effectiveness of the proposed secondary control

17518695, 2022, 5, Downloaded from https://ietresearch.onlinelibrary.wiley.com/doi/10.1049/gtd2.12345 by Readcube (Labtiva Inc.), Wiley Online Library on [04/11/2022]. See the Terms and Conditions (https://onlinelibrary.wiley.com/terms-and-conditions) on Wiley Online Library for rules of use; OA articles are governed by the applicable Creative Commons License

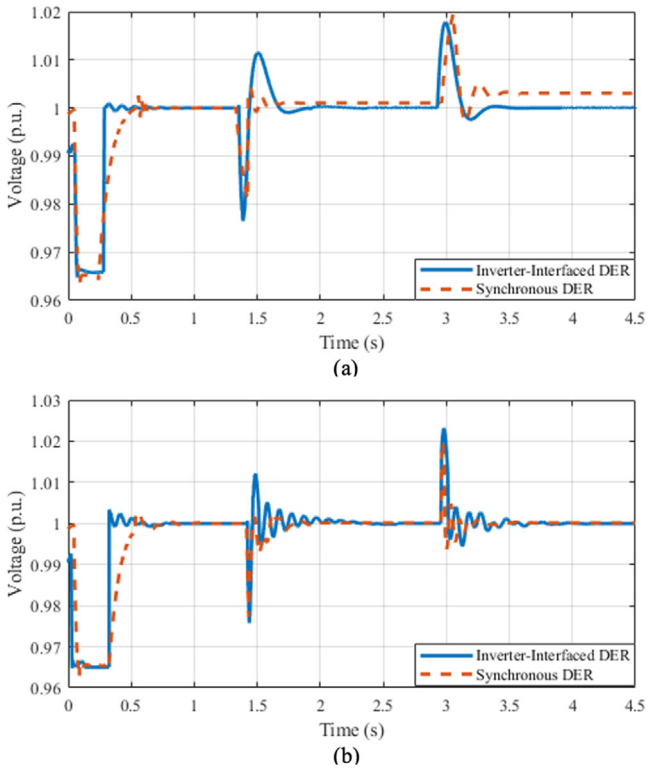

FIGURE 5 Performance and robustness evaluation (a) $h = 3$, (b) $h = 5$

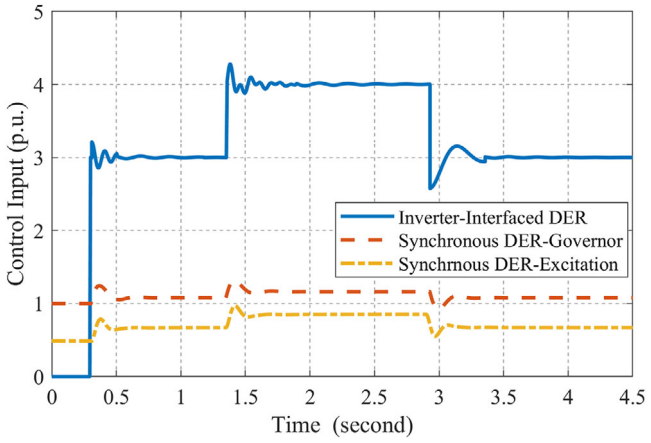

FIGURE 6 Control inputs for h = 3

method. To this aim, the proposed RFMPC method is evaluated under two different upper bounds of the time-varying communication delays $h = 3$ (or equivalently 300 ms) and $h = 5$ (or equivalently 500 ms). The confidence levels for $h = 3$ are chosen as $\gamma_0 = 0.7, \gamma_{-1} = 0.1, \gamma_{-2} = 0.1$, and $\gamma_{-3} = 0.1$; and for $h = 5$, they are selected as $\gamma_0 = 0.8$, $\gamma_{-1} = 0.1, \gamma_{-2} = 0.05, \gamma_{-3} = 0.02, \gamma_{-4} = 0.02$, and $\gamma_{-5} = 0.01$. Note that the confidence levels are selected deliberately to fulfill the above two constraints. The uncertainty of μG parameters (including the impedances of lines and DERs) is considered 20%. The scenario under study is simulated as follows:

1. $t = 0.0$ s (simulation initialization period): μG works on the islanded mode, and only the primary control is activated.
2. $t = 0.3$ s: The proposed secondary control comes into the operation.
3. $t = 1.35$ s: Load 1 is increased by 30%.
4. $t = 2.9$ s: Load 1 in step 3 is decreased to its nominal value.

The simulation results are depicted in Figure 5. Firstly, the effectiveness of the proposed secondary voltage control is validated considering $h = 3$ for communication delays and Figure 5a illustrates the DERs' terminal voltage amplitudes for this case. At $t = 0$, the simulation is started. During the first stage, only the primary local control is activated for each DER. The DERs' terminal voltage amplitudes, v_i, are deviated from their reference values by their primary controllers. Consequently, the μG's voltages need to be restored at the secondary hierarchy control level of the μG. Once the proposed secondary control is undertaken at $t = 0.3$ s, the deviated voltages converge to their pre-specified reference values in 0.22 and 0.20 s for the synchronous and inverter-interfaced DERs respectively. Note that the settling time, in this paper, is defined as a period of time in which oscillations are completely removed and the deviated voltages converge to their setpoint (e.g. $v_{ref} = 1 p.u.$).

Now the performance of the proposed RFMPC scheme against load uncertainty is investigated. For this sake, Load 1 is increased and decreased by 30% at $t = 1.35$ s and $t = 2.9$ s, respectively. The increment and decrement of Load 1 have occurred abruptly. Figure 5a confirms that the proposed secondary controller demonstrates decent tracking and robust performance against the load severe changes and accurately restores the DERs' output voltages.

Second, in order to investigate the influence of large time delays on the practical performance, the communication delay between μG central control and DERs is considered to be $h = 5$ and the results are shown in Figure 5b. Without further explanations, the performance evaluation of $h = 5$ is similar to that of $h = 3$. The main difference between the two cases is that further latency might slightly weaken the controller performance in terms of oscillations and settling time.

In what follows, we evaluate control inputs for both inverter-interfaced and synchronous DERs. Note that in order to avoid repetition and due to the lack of enough space, we assess control signals only for $h = 3$. Control inputs are depicted in Figure 6. According to this figure, it can be seen that all of the control inputs are lower than their maximum values. Also, since the inertia of inverter-based DER is lower than that of synchronous one, it plays important role in the secondary control of the μG. The RMS value of control inputs are: 3.2955 for inverter-interfaced DER, 0.7273 for the governor of synchronous DER, and 1.1084 for the excitation systems of synchronous DER. As a result, it is obvious that using the proposed method, the control signals never violate their limits.

17518695, 2022, 5, Downloaded from https://ietresearch.onlinelibrary.wiley.com/doi/10.1049/gtd2.12345 by Readcube (Labtiva Inc.), Wiley Online Library on [04/11/2022]. See the Terms and Conditions (https://onlinelibrary.wiley.com/terms-and-conditions) on Wiley Online Library for rules of use; OA articles are governed by the applicable Creative Commons License

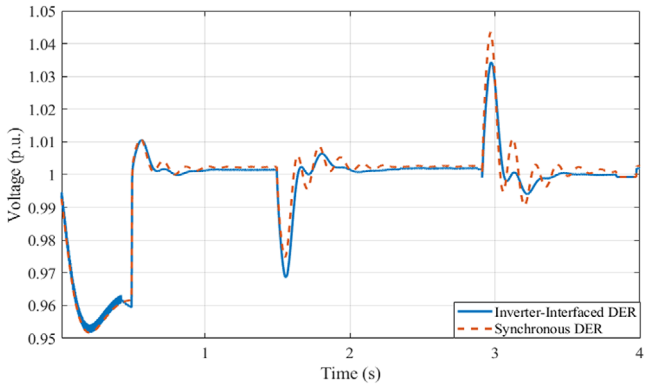

FIGURE 7 Evaluation of proposed method under severe variation of communication deficiency and μG uncertainty

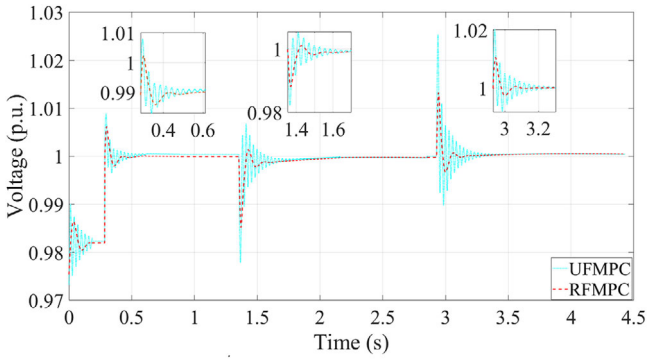

FIGURE 8 Comparison between the proposed secondary voltage control and UFMPC methods

4.2 | System performance under severe variation of communication deficiencies and μG uncertainties

To evaluate the proposed method performance under the varying communication deficiencies and μG uncertainties, the following changes are applied to the previous case study:

1. The variance of noises is increased to $\eta = 0.5$;
2. Time delay is increased to $h = 7$ (or equivalently 700 ms);
3. μG parameter uncertainties are increased to 50%;
4. The amount of increasing/decreasing of Load 1 is considered 50%.

Confidence levels are chosen as $\gamma_0 = 0.6, \gamma_{-1} = 0.15$, $\gamma_{-2} = 0.1, \gamma_{-3} = 0.07, \gamma_{-4} = 0.04, \gamma_{-5} = 0.025, \gamma_{-6} = 0.01$, and $\gamma_{-7} = 0.005$. The obtained simulation results are illustrated in Figure 7. In this study case, it is seen that the proposed method can still restore the DERs' voltages to their nominal values under extreme conditions. However, a longer transient time and slower convergence speed for DERs are observed. For instance, the settling time of DER1 at the moment of increasing the uncertainty of Load 1 in Case A was less than 0.3 s; however, this value prolongs up to 0.5 s in Case B for the same DER. Similarly, the maximum overshoot in the voltage response in Case A is 0.022; however, it is greater than 0.045 in Case B. In this study, it is illustrated that under severe circumstances, not only does our proposed method remain stable, but also the maximum obtained overshoot is less than the critical value of 5%.

4.3 | Comparison of RFMPC with the method proposed in [31]

In this case, we compare the proposed RFMPC method with a previously-discussed secondary control approach in [31], in which the authors proposed a new unified FMPC (UFMPC) scheme in order to regulate voltage in islanded μG by considering fixed time delay and disturbances. The previous scenario of Case A is performed using both UFMPC and RFMPC methods. The delay values are chosen as four samples in the communication network ($h = 4$ or equivalently 400 ms). The voltage responses obtained from the two methods are compared in Figure 8. For the sake of brevity, only voltage responses of DER1 are depicted. In comparison with the UFMPC, RFMPC shrinks the settling time and overshoot; thus, it exhibits a better control performance. In Figure 7, it is observed that the proposed RFMPC can keep voltages within the remarkable precision. The proposed method yields better disturbance rejection and time delay treatment.

TABLE 2 Comparison of computation burden

Method	Average time
UFMPC Method	1.5943s/step
Proposed RFMPC	0.5456s/step

The computation burden for those two different strategies are given in Table 2 under the same hardware and software specifications. It can be seen that, compared with the proposed scheme, the computational burden of UFMPC is much heavier. The reason lies in that the proposed RFMPC method includes two different offline and online stages. In the offline stage, an optimal region and a sequence of terminal constraint sets are derived through solving a BMI problem, while the online stage consists of solving an LMI problem, which is not very complex. As a result, the computation burden is dramatically reduced in comparison to that of the UFMPC method. According to the comparative study, it can be easily seen that our proposed method has superior dynamic features compared to the previous work [31]. For example, the overshoot and the settling time of the proposed method are lower than those of [31]. Also, in this subsection, we showed that our proposed method can reduce the computation burden by a factor of almost 1/3. Our proposed method is interesting for operators since, in order to save cost, they do not prefer high computational systems, which lead to an increase in the computation burden dramatically. However, according to the obtained computation burden, our proposed method can reduce computation process time to a

17518695, 2022, 5, Downloaded from https://ietresearch.onlinelibrary.wiley.com/doi/10.1049/gtd2.12345 by Readcube (Labtiva Inc.), Wiley Online Library on [04/11/2022]. See the Terms and Conditions (https://onlinelibrary.wiley.com/terms-and-conditions) on Wiley Online Library for rules of use; OA articles are governed by the applicable Creative Commons License

great extent considering the same computer system. As a result, operators do not need high-speed, expensive computers.

5 | CONCLUSIONS AND FUTURE WORK

In this article, a RFMPC method for voltage restoration in islanded μGs concerning time-varying communication delays and credible uncertainties and disturbances is proposed. The implementation of the proposed method includes both offline and online computation stages. In the offline stage, based on the LRF approach, a sequence of control laws related to a sequence of robust constraint sets are computed, while the online computation stage includes solving a convex optimization problem with LMI constraints. The simulation results verified that the proposed method: (1) Robustly restores the voltage magnitudes of the whole μG to their reference values in the presence of the communication delay, uncertainty, and disturbances; (2) demonstrates robust performance even in the presence of larger time delays and greater disturbances; and (3) has privileges in control performance and computational burden.

FUNDING
None.

CONFLICT OF INTEREST STATEMENT
None

PERMISSION TO REPRODUCE MATERIALS FROM OTHER SOURCES
None

DATA AVAILABILITY STATEMENT
The data that support the findings of this study are available by requesting from the corresponding author upon a reasonable request.

ORCID
Masood Mottaghizadeh https://orcid.org/0000-0001-9175-7209
Farrokh Aminifar https://orcid.org/0000-0003-2331-2798

REFERENCES
1. Bidram, A., Davoudi, A., Lewis, F.L., et al.: Secondary controlof microgrids based on distributed cooperative control of multi-agent systems. IET Gener. Transm. Distrib. 8(7), 822–831 (2013)
2. Gómez, J.S., Sáez, D., Simpson-Porco, J.W., Cárdenas, R.: Distributed predictive control for frequency and voltage regulation in microgrids. IEEE Trans. Smart Grid 2(11), 1319–1329 (2020)
3. Lou, G., Gu, W., Xu, Y., Cheng, M., Liu, W.: Distributed MPC-based secondary voltage control scheme for autonomous droop-controlled microgrids. IEEE Trans. Sustainable Energy 8(2), 792–804 (2017)
4. Babayomi, O., Li, Z., Zhang, Z.: Distributed secondary frequency and voltage control of parallel-connected vscs in microgrids: A predictive VSG-based solution. CPSS Trans. Power Electron. App. 5(4), 342–351 (2020)
5. Subramanian, L., Debusschere, V., Gooi, H.B., Hadjsaid, N.: A cooperative rate-based model predictive framework for flexibility management of DERs. IEEE Trans. Energy Conver. (2021) https://doi.org/10.1109/TEC.2021.3105612
6. Babqi, A., Yi, Z., Etemadi, A.H.: Centralized finite control set model predictive control for a multiple distributed generators small-scale microgrid. In: *2017 North American Power Symposium (NAPS)*, Morgantown, WV, USA, pp. 1–5 (2017)
7. Zamora, R., Srivastava, A.K.: Multi-layer architecture for voltage and frequency control in networked microgrids. IEEE Trans. Smart Grid 9(3), 2076–2085 (2018)
8. Ahumada, C., Cardenas, R., Saez, D., Guerrero, J.M.: Secondary control strategies for frequency restoration in islanded microgrids with consideration of communication delays. IEEE Trans. Smart Grid 7(3), 1430–1441 (2016)
9. Chen, T., Abdel-Rahim, O., Peng, F., Wang, H., An improved finite control set-MPC-based power sharing control strategy for islanded AC microgrids. IEEE Access 8, 52676–52686 (2020)
10. Lou, G., Gu, W., Xu, Y., et al.: Stability robustness for secondary voltage control in autonomous microgrids with consideration of communication delays. IEEE Trans. Power Syst. 33(4), 4164–4178 (2018)
11. Zhao, Z., et al.: Decentralized finite control set model predictive control strategy of microgrids for unbalanced and harmonic power management. IEEE Access 8, 202298–202311 (2020)
12. Zheng, C., Dragičević, T., Zhang, Z., Rodriguez, J., Blaabjerg, F.: Model predictive control of LC-filtered voltage source inverters with optimal switching sequence. IEEE Trans. Power Electron. 36(3), 3422–3436 (2021)
13. Sahoo, S., Blaabjerg, F.: A model-free predictive controller for networked microgrids with random communication delays. In: 2021 *IEEE Applied Power Electronics Conference and Exposition (APEC)*, Phoenix, AZ, USA, pp. 2667–2672 (2021)
14. Ma, D., et al.: Dual-predictive control with adaptive error correction strategy for AC microgrids. IEEE Trans. Power Delivery (2021) https://doi.org/10.1109/TPWRD.2021.3101198
15. Habibi, M.R., Baghaee, H.R., Blaabjerg, F., Dragicevic, T.: Secure MPC/ANN-based false data injection cyber-attack detection and mitigation in DC microgrids. IEEE Syst. J., https://doi.org/10.1109/JSYST.2021.3086145
16. Yao, W., Wang, Y., Xu, Y., Deng, C., Wu, Q.: Distributed Weight-average-prediction control and stability analysis for an islanded microgrid with communication time delay. IEEE Trans. Power Syst., https://doi.org/10.1109/TPWRS.2021.3092717
17. Ahumada, C., Cárdenas, R., Sáez, D., Guerrero, J.M.: Secondary control strategies for frequency restoration in islanded microgrids with consideration of communication delays. IEEE Trans. Smart Grid 7(3), 1430–1441 (2016)
18. Heydari, R., Khayat, Y., Amiri, A., et al.: Robust high-rate secondary control of microgrids with mitigation of communication impairments. IEEE Trans. Power Electron. 35(11), 12486–12496 (2020)
19. Seyedi, Y., Karimi, H., Guerrero, J.M.: Centralized disturbance detection in smart microgrids with noisy and intermittent synchrophasor data. IEEE Trans. Smart Grid 8(6), 2775–2783 (2017)
20. Patrao, I., González-Medina, R., Marzal, S., et al.: Synchronization of power inverters in islanded microgrids using an FM-modulated signal. IEEE Trans. Smart Grid 8(1), 503–510 (2017)
21. Olama, A., Mendes, P.R.C., Camacho, F.: Lyapunov-based hybrid model predictive control for energy management of microgrids. IET Gener. Transm. Distrib. 12(21), 5770-5780 (2018)
22. Li, D., Xi, Y.: Constrained feedback robust model predictive control for polytopic uncertain systems with time delays. Int. J. Syst. Sci. 42(10), 1651–1660 (2011)
23. Lu, J., Li, D., Xi, Y.: Probability-based constrained MPC for structured uncertain systems with state and random input delays. Int. J. Syst. Sci. 44(7), 1354–1365 (2013)
24. Raimondi Cominesi, S., Farina, M., Giulioni, L., Picasso, B., Scattolini, R.: A two-layer stochastic model predictive control scheme for microgrids. IEEE Trans. Control Syst. Technol. 26(1), 1–13 (2018)
25. Novoselnik, B., Matuško, J., Baoti´c, M.: Robust microgrid control using tube scaling approach. In: *Proceedings of the 2017 American Control Conference (ACC)*, Seattle, WA, USA, pp. 767–772 (2017)

17518695, 2022, 5, Downloaded from https://ietresearch.onlinelibrary.wiley.com/doi/10.1049/gtd2.12345 by Readcube (Labtiva Inc.), Wiley Online Library on [04/11/2022]. See the Terms and Conditions (https://onlinelibrary.wiley.com/terms-and-conditions) on Wiley Online Library for rules of use; OA articles are governed by the applicable Creative Commons License

26. Zhang, J., Li, L., Dorrell, D.G., Norambuena, et al.: Predictive voltage control of direct matrix converters with improved output voltage for renewable distributed generation. IEEE J. Emerg. Sel. Topics Power Electron. 7(1), 296–308 (2019)
27. Wei, Y., Qiu, J., Shi, P., *et al.*: A piecewise-markovian lyapunov approach to reliable output feedback control for fuzzy-affine systems with time-delays and actuator faults. IEEE Trans. Cyber. 48(9), 2723–2735 (2018)
28. Wei, Y., Qiu, J., Lam, H.K., *et al.*: Approaches to T-S fuzzy affine model based reliable output feedback control for non-linear ito stochastic systems. IEEE Trans. Fuzzy Syst. 25(3), 569–583 (2017)
29. Hosseinalizadeh, T., Kebriaei, H., Salmasi, F.R.: Decentralised robust T-S fuzzy controller for a parallel islanded AC microgrid. IET Gener. Transm. Distrib. 13(9), 1589–1598 (2019)
30. Jiang, H., Lin, J., Song, Y., et al.: Explicit model predictive control applications in power systems: An AGC study for an isolated industrial system. IET Gener. Transm. Distrib 10(4), 964–971 (2016)
31. Shan, X.Y., Hu, J., Chan, K.W., et al.: A unified model predictive voltage and current control for microgrids with distributed fuzzy cooperative secondary control. IEEE Trans. Ind. Inform. 17(12), 8024–8034 (2021)
32. Zhu, J., Nguang, S.K.: Fuzzy model predictive control with enhanced robustness for nonlinear system via a discrete disturbance observer. IEEE Access 8, 220631–220645 (2020)
33. Mottaghizadeh, M., Aminifar, F., Amraee, T., Sanaye-Pasand, M.: Distributed robust secondary control of islanded microgrids: voltage, frequency, and power sharing. IEEE Trans. Power Delivery 36(4), 2501–2509 (2021)
34. Kundur, P., Balu, N.J., Lauby, M.G.: Power System Stability and Control, 1st ed.. McGraw-Hill, New York (1994)
35. Wang, J., Liu, Y., Li, H., 'Finite-time controllability and set controllability of impulsive probabilistic boolean control networks. IEEE Access 8, 111995–112002 (2020)
36. Katiraei, F., Iravani, M.R., Lehn, P.W.: Small-signal dynamic model of a micro-grid including conventional and electronically interfaced distributed resources. IET Gener. Transm. Distrib. 1(3), 369–378 (2007)
37. Su, Y., Shi, Y., Sun, C.: Distributed model predictive control for tracking consensus of linear multiagent systems with additive disturbances and time-varying communication delays. IEEE Trans. Cyber 51(7), 3813–3823 (2021)

How to cite this article: Mottaghizadeh, M., Aminifar, F., Amraee, T., Sanaye-Pasand, M.: Robust fuzzy model predictive control for voltage regulation in islanded microgrids. IET Gener. Transm. Distrib. 16, 1013–1029 (2022). https://doi.org/10.1049/gtd2.12345

APPENDIX A

Definition 1 (LRF-type RPI Set) [20]. *For the considered discrete-time non-linear DDI by (13), a set* $\Omega \subseteq \mathbb{R}^n$ *is called an RPI set for the closed-loop system with the feedback control law* π, *if* $\mathbf{y}(k+1) \in \Omega$, *for all* $\mathbf{y}_{[k-b,k]} \in \Omega^{b+1}$ *and* $\forall \mathbf{w} \in \mathbb{W}$, $\mathbb{W} \subseteq \mathbb{R}^e$ *holds.*

Definition 2 (ISS) [33, 37]. *The DDI (13) is called ISS if there exists a* $\mathcal{KL}$*-class function* β *and a* $\mathcal{K}$*-class function* σ, *such that for all* $k \in \mathbb{Z}_+$ *it holds that:*

$$\|\mathbf{y}(k)\| \leq \beta\left(\|\mathbf{y}(0)\|, k\right) + \sigma\left(\|\mathbf{w}\|\right) \tag{A1}$$

where $\mathbf{y}(0)$ *represents the initial state value.*

APPENDIX B

In this appendix, the terminal constraint set is acquired. The terminal constraint set should satisfy the following two conditions. Firstly, it should be an RPI set. To do so, define a positive definite function $V(\mathbf{y}) := (\mathbf{y}-\mathbf{y}_r)^T \mathbf{P}_t (\mathbf{y}-\mathbf{y}_r)$ and $\Omega_t \subseteq \mathbb{R}^n$ as a terminal constraint set for RFMPC problem as:

$$\Omega_t := \{\mathbf{y} | \bar{V}(\mathbf{y}(k)) \leq \xi\} \tag{B1}$$

where $\xi > 0$ is a constant scalar, which will be computed later and $\bar{V}(\mathbf{y}(k)) = \max_{i \in \mathbb{Z}_{[-b,0]}} \{V(\mathbf{y}(k+i) - \mathbf{y}_r(k+i))\}$. From the definition of the Lyapunov functions $V(\mathbf{y})$ and $\bar{V}(\mathbf{y})$, it can be seen that Ω_t is a convex set. The first requirement is given in the following lemma.

Lemma 1. *The set* Ω_t *in* (B1) *is an RPI set for the considered* μG *in* (16), *if there exists a positive scalar* $\lambda \in \mathbb{R}_{(0,1)}$ *such that:*

$$\frac{1}{\xi} V\left(\mathbf{y}^+ - \mathbf{y}_r^+\right) - \frac{1-\lambda}{\xi} \bar{V}(\mathbf{y}(k) - \mathbf{y}_r(k)) - \frac{\lambda}{\eta^2} \mathbf{w}^T(k)\mathbf{w}(k) \leq 0 \tag{B2}$$

where $\mathbf{y}^+, \mathbf{y}_r^+$ represent respectively the value of $\mathbf{y}, \mathbf{y}_r$ at the next time instant, k+1.

Secondly, the terminal constraint set should satisfy the ISS property. This condition implies that there exists two $\mathcal{K}_\infty$-class functions α_3,α_4 and a positive definite function $V(\mathbf{y})$ such that $\forall \mathbf{y} \in \Omega_t$:

$$\alpha_3(\|\mathbf{y}-\mathbf{y}_r\|) \leq V(\mathbf{y}) \leq \alpha_4(\|\mathbf{y}-\mathbf{y}_r\|) \tag{B3a}$$

$$\begin{aligned} &V\left(\mathbf{y}^+ - \mathbf{y}_r^+\right) - \bar{V}(\mathbf{y}(k) - \mathbf{y}_r(k)) \leq \\ &-(\mathbf{y}(k) - \mathbf{y}_r(k))^T \mathbf{Q}(\mathbf{y}(k) - \mathbf{y}_r(k)) - \mathbf{u}^T(k)\mathbf{R}\mathbf{u}(k) \\ &-\psi \mathbf{w}^T(k+s|k)\mathbf{w}(k+s|k) \end{aligned} \tag{B3b}$$

Now the two aforementioned conditions are provided in the form of matrix inequalities.

Theorem 2. *For the considered* μG *representation in (16), the set (B1) is an RPI set with respect to the corresponding feedback control law* π_t, *if there exists a positive definite matrix* $\mathbf{X}_t$, *general matrices* $\mathbf{Y}_a$, $\mathbf{Y}_b$, $\mathbf{Y}_l$, $\mathbf{Z}$, $\mathbf{G}_b$ *and two positive scalars* ψ, $\lambda \in \mathbb{R}_{(0,1)}$, *such that the following three matrix inequalities are feasible* [33]:

$$\begin{bmatrix} \mathbf{\Psi}_0 & \mathbf{0} & \cdots & \mathbf{0} & \mathbf{0} & \mathbf{\Pi}_0^T \\ \mathbf{0} & \mathbf{\Psi}_1 & \cdots & \cdots & \cdots & \mathbf{\Pi}_1^T \\ \vdots & \vdots & \ddots & \vdots & \vdots & \vdots \\ \mathbf{0} & \mathbf{0} & \cdots & \mathbf{\Psi}_b & \mathbf{0} & \mathbf{\Pi}_b^T \\ \mathbf{0} & \mathbf{0} & \cdots & \mathbf{0} & -\frac{\lambda}{\eta^2} I & \mathbf{E}_a^T \\ \mathbf{\Pi}_0 & \mathbf{\Pi}_1 & \cdots & \mathbf{\Pi}_b & \mathbf{E}_a & -\mathbf{X}_t \end{bmatrix} \leq 0 \tag{B4a}$$

17518695, 2022, 5, Downloaded from https://ietresearch.onlinelibrary.wiley.com/doi/10.1049/gtd2.12345 by Readcube (Labtiva Inc.), Wiley Online Library on [04/11/2022]. See the Terms and Conditions (https://onlinelibrary.wiley.com/terms-and-conditions) on Wiley Online Library for rules of use; OA articles are governed by the applicable Creative Commons License

$$\begin{bmatrix} \boldsymbol{\Phi}_0 & \mathbf{0} & \cdots & \mathbf{0} & \mathbf{0} & \boldsymbol{\Pi}_0^T & (\mathbf{QX}_e)^T & (\mathbf{RY}_b)^T \\ \mathbf{0} & \boldsymbol{\Phi}_1 & \cdots & \cdots & \mathbf{0} & \boldsymbol{\Pi}_1^T & \mathbf{0} & \mathbf{0} \\ \vdots & \vdots & \ddots & \vdots & \vdots & \vdots & \vdots & \vdots \\ \mathbf{0} & \mathbf{0} & \cdots & \boldsymbol{\Phi}_b & \mathbf{0} & \boldsymbol{\Pi}_b^T & \mathbf{0} & \mathbf{0} \\ \mathbf{0} & \mathbf{0} & \cdots & \mathbf{0} & -\psi\xi\boldsymbol{I} & \left(\xi\mathbf{E}_a\right)^T & \mathbf{0} & \mathbf{0} \\ \boldsymbol{\Pi}_0 & \boldsymbol{\Pi}_1 & \cdots & \boldsymbol{\Pi}_b & \xi\boldsymbol{E}_a & -\mathbf{X}_t & \mathbf{0} & \mathbf{0} \\ \mathbf{QX}_e & \mathbf{0} & \cdots & \mathbf{0} & \mathbf{0} & \mathbf{0} & -\xi\mathbf{Q} & 0 \\ \mathbf{RY}_b & \mathbf{0} & \cdots & \mathbf{0} & \mathbf{0} & \mathbf{0} & \mathbf{0} & -\xi\mathbf{R} \end{bmatrix} \leq 0 \tag{B4b}$$

$$\begin{bmatrix} \mathbf{Z} & \mathbf{Y}_b \\ \mathbf{Y}_b^T & \mathbf{G}_b + \mathbf{G}_b^T - \mathbf{X}_t \end{bmatrix} \geq 0, \mathbf{Z}_{tt} \leq \mathbf{u}_{t,max}^2, \quad t \in \mathbb{Z}_{[0,m]} \tag{B4c}$$

where $\mathbf{0}$ and $\boldsymbol{I}$ are the zero and identity matrices; $a, b \in \mathbb{Z}_{[1,L]}$, $\mathbf{Z}_{tt}$ is the t^{th} diagonal element of matrix $\mathbf{Z}$; $\boldsymbol{\Psi}_{-i} = -\gamma_i(1-\lambda)(\mathbf{G}_b + \mathbf{G}_b^T - \mathbf{X}_t)$, $\boldsymbol{\Phi}_{-i} = -\gamma_i(\mathbf{G}_b + \mathbf{G}_b^T - \mathbf{X}_t)$, $i \in \mathbb{Z}_{[-b,0]}$, γ_i are positive numbers; $\boldsymbol{\Pi}_0 = \mathbf{A}_{0,a}\mathbf{X}_e + \mathbf{B}_a\mathbf{Y}_b$, $\boldsymbol{\Pi}_{-j} = \mathbf{A}_{j,a}\mathbf{X}_t$, $j \in \mathbb{Z}_{[-b,-1]}$; $\mathbf{P}_t = \xi\mathbf{X}_t^{-1}$; $\pi_t = \mathbf{K}_\mu\mathbf{y}$, with $\mathbf{K}_\mu = \sum_{l=1}^{L}\mu_l K_l$ and $\mathbf{K}_l = \mathbf{Y}_l\mathbf{X}_e^{-1}$.

Proof. First, we demonstrate that (B5) implies (B4a). Toward this end, resorting to the dilation lemma [37],

$$-\mathbf{G}_b^T\mathbf{X}_t^{-1}\mathbf{G}_b \leq \mathbf{X}_t - \mathbf{G}_b - \mathbf{G}_b^T \tag{B5}$$

The following inequality is obtained from (B5),

$$\begin{bmatrix} \mathbf{M}_0 & \mathbf{0} & \cdots & \mathbf{0} & \mathbf{0} & \boldsymbol{\Pi}_0^T \\ \mathbf{0} & \mathbf{M}_1 & \cdots & \cdots & \cdots & \boldsymbol{\Pi}_1^T \\ \vdots & \vdots & \ddots & \vdots & \vdots & \vdots \\ \mathbf{0} & \mathbf{0} & \cdots & \mathbf{M}_b & \mathbf{0} & \boldsymbol{\Pi}_b^T \\ \mathbf{0} & \mathbf{0} & \cdots & \mathbf{0} & -\frac{\lambda}{\eta^2}\boldsymbol{I} & \mathbf{E}_a^T \\ \boldsymbol{\Pi}_0 & \boldsymbol{\Pi}_1 & \cdots & \boldsymbol{\Pi}_b & \mathbf{E}_a & -\mathbf{X}_t \end{bmatrix} \leq 0 \tag{B6}$$

where $\mathbf{M}_{-i} = \gamma_i(\lambda-1)\mathbf{G}_b^T\mathbf{X}_t^{-1}\mathbf{G}_b$. By multiplying $\text{diag}\{\mathbf{G}_b^{-T}, \mathbf{G}_b^{-T}, \ldots, \mathbf{G}_b^{-T}, I, I\}$ and its transpose from both sides of (B6), respectively, yields that

$$\begin{bmatrix} \boldsymbol{\Delta}_0 & \mathbf{0} & \cdots & \mathbf{0} & \mathbf{0} & \boldsymbol{\Pi}_0^T \\ \mathbf{0} & \boldsymbol{\Delta}_1 & \cdots & \cdots & \cdots & \boldsymbol{\Pi}_1^T \\ \vdots & \vdots & \ddots & \vdots & \vdots & \vdots \\ \mathbf{0} & \mathbf{0} & \cdots & \boldsymbol{\Delta}_b & \mathbf{0} & \boldsymbol{\Pi}_b^T \\ \mathbf{0} & \mathbf{0} & \cdots & \mathbf{0} & -\frac{\lambda}{\eta^2}\boldsymbol{I} & \mathbf{E}_a^T \\ \tilde{\mathbf{A}}_0 & \tilde{\mathbf{A}}_{-1} & \cdots & \tilde{\mathbf{A}}_{-b} & \mathbf{E}_a & -\mathbf{X}_t \end{bmatrix} \leq 0 \tag{B7}$$

where $\boldsymbol{\Delta}_{-i} = \gamma_i(\lambda-1)\mathbf{X}_t^{-1}$, $\tilde{\mathbf{A}}_0 = \mathbf{A}_{0,a} + \mathbf{B}_a K_b$, $\tilde{\mathbf{A}}_j = \mathbf{A}_{j,a}$, $j \in \mathbb{Z}_{[-b,-1]}$. Based on which one can obtain

$$\sum_{a=1}^{L}\sum_{b=1}^{L}\mu_a\mu_b \begin{bmatrix} \boldsymbol{\Delta}_0 & \mathbf{0} & \cdots & \mathbf{0} & \mathbf{0} & \boldsymbol{\Pi}_0^T \\ \mathbf{0} & \boldsymbol{\Delta}_1 & \cdots & \cdots & \cdots & \boldsymbol{\Pi}_1^T \\ \vdots & \vdots & \ddots & \vdots & \vdots & \vdots \\ \mathbf{0} & \mathbf{0} & \cdots & \boldsymbol{\Delta}_b & \mathbf{0} & \boldsymbol{\Pi}_b^T \\ \mathbf{0} & \mathbf{0} & \cdots & \mathbf{0} & -\frac{\lambda}{\eta^2}\boldsymbol{I} & \mathbf{E}_a^T \\ \tilde{\mathbf{A}}_0 & \tilde{\mathbf{A}}_{-1} & \cdots & \tilde{\mathbf{A}}_{-b} & \mathbf{E}_\mu & -\mathbf{X}_t \end{bmatrix} \leq 0 \tag{B8}$$

where $\sum_{a=1}^{L}\mu_a = 1$, $\sum_{b=1}^{L}\mu_b = 1$. The above inequality can be written as follows:

$$\begin{bmatrix} \boldsymbol{\Delta}_0 & \mathbf{0} & \cdots & \mathbf{0} & \mathbf{0} & \boldsymbol{\Pi}_0^T \\ \mathbf{0} & \boldsymbol{\Delta}_1 & \cdots & \cdots & \cdots & \boldsymbol{\Pi}_1^T \\ \vdots & \vdots & \ddots & \vdots & \vdots & \vdots \\ \mathbf{0} & \mathbf{0} & \cdots & \boldsymbol{\Delta}_b & \mathbf{0} & \boldsymbol{\Pi}_b^T \\ \mathbf{0} & \mathbf{0} & \cdots & \mathbf{0} & -\frac{\lambda}{\eta^2}\boldsymbol{I} & \mathbf{E}_a^T \\ \tilde{\mathbf{A}}_{0,\mu} & \tilde{\mathbf{A}}_{-1,\mu} & \cdots & \tilde{\mathbf{A}}_{-b,\mu} & \mathbf{E}_\mu & -\mathbf{X}_t \end{bmatrix} \leq 0 \tag{B9}$$

where $\tilde{\mathbf{A}}_{0,\mu} = \mathbf{A}_{0,\mu} + \mathbf{B}_\mu K_\mu$, $\tilde{\mathbf{A}}_{j,\mu} = \mathbf{A}_{j,\mu}$, $j \in \mathbb{Z}_{[-b,-1]}$. Applying the Schur complement to (B9), and then multiplying $[\mathbf{y}^T(k), \mathbf{y}^T(k-1), \ldots, \mathbf{y}^T(k-h), \mathbf{w}^T(k)]$ and its transpose from both sides of the resulting matrix inequality, respectively, yields that

$$\boldsymbol{\varpi}\begin{bmatrix} \boldsymbol{\Delta}_0 & \mathbf{0} & \cdots & \mathbf{0} & \mathbf{0} \\ \mathbf{0} & \boldsymbol{\Delta}_1 & \cdots & \mathbf{0} & \mathbf{0} \\ \vdots & \vdots & \ddots & \vdots & \vdots \\ \mathbf{0} & \mathbf{0} & \cdots & \boldsymbol{\Delta}_b & \mathbf{0} \\ \mathbf{0} & \mathbf{0} & \cdots & \mathbf{0} & -\frac{\lambda}{\eta^2}\boldsymbol{I} \end{bmatrix}\boldsymbol{\varpi}^T + \boldsymbol{\varpi}\boldsymbol{\Lambda}\mathbf{X}_t^{-1}\boldsymbol{\Lambda}^T\boldsymbol{\varpi}^T \leq 0 \tag{B10}$$

where $\boldsymbol{\varpi} = [\mathbf{y}^T(k), \mathbf{y}^T(k-1), \ldots, \mathbf{y}^T(k-h), \mathbf{w}^T(k)]$, $\boldsymbol{\Lambda} = [\tilde{\mathbf{A}}_{0,\mu}, \tilde{\mathbf{A}}_{-1,\mu}, \ldots, \tilde{\mathbf{A}}_{-b,\mu}, \mathbf{E}_\mu]^T$. By substituting $\mathbf{X}_t^{-1}$ with $\mathbf{P}_t/\zeta$, (B10) is equal to

$$\begin{aligned} &(\lambda-1)\sum_{i=-b}^{0}\gamma_i\mathbf{y}^T(k+i)\mathbf{X}_t^{-1}\mathbf{y}(k+i) - \frac{\lambda}{\eta^2}\mathbf{w}^T(k)\mathbf{w}(k) \\ &+ \left(\sum_{i=-b}^{0}\mathbf{y}^T(k+i)\left(\tilde{\mathbf{A}}_{-i,\mu}\right)^T\right)\mathbf{X}_t^{-1}\left(\sum_{i=-b}^{0}\mathbf{y}^T(k+i)\left(\tilde{\mathbf{A}}_{-i,\mu}\right)^T\right)^T \\ &= \frac{(\lambda-1)}{\xi}\sum_{i=-b}^{0}\gamma_i\mathbf{y}^T(k+i)\mathbf{P}_t\mathbf{y}(k+i) - \frac{\lambda}{\eta^2}\mathbf{w}^T(k)\mathbf{w}(k) + \frac{1}{\xi}\mathbf{y}^{+T}\mathbf{P}_t\mathbf{y}^+ \\ &= \frac{(\lambda-1)}{\xi}\sum_{i=-b}^{0}\gamma_i\mathrm{V}\left(\mathbf{y}(k+i)\right) - \frac{\lambda}{\eta^2}\mathbf{w}^T(k)\mathbf{w}(k) + \frac{1}{\xi}\mathrm{V}\left(\mathbf{y}^+\right) \leq 0 \end{aligned} \tag{B11}$$

Since $\sum_{i=-b}^{0}\gamma_i = 1$, it is easy to get $\sum_{i=-b}^{0}\gamma_i\mathrm{V}(\mathbf{y}(k+i)) \leq \bar{\mathrm{V}}(\mathbf{y}^+)$. Therefore, (B4a) is obtained. Note that the obtained

17518695, 2022, 5, Downloaded from https://ietresearch.onlinelibrary.wiley.com/doi/10.1049/gtd2.12345 by Readcube (Labtiva Inc.), Wiley Online Library on [04/11/2022]. See the Terms and Conditions (https://onlinelibrary.wiley.com/terms-and-conditions) on Wiley Online Library for rules of use; OA articles are governed by the applicable Creative Commons License

terminal constraint is not necessarily optimal; therefore, in this paper, we acquired an optimal region for the convergence of the proposed method. It should be noted that (B4b) can be easily got by resorting to the eigenvalues of $\mathbf{P}_t$. In order to prevent repetition, it is not mentioned.

Define invariance set $\mathcal{V}$ as follows:

$$\left\{v|v^T\mathbf{X}_t^{-1}v \le 1\right\} \tag{B12}$$

Now we consider the input constraints as follows:

$$\left|\mathbf{u}_t(k+i|k)\right| \le \mathbf{u}_{t,max}, \quad t \in \mathbb{Z}_{[0,m]} \tag{B13}$$

It can be also described as $|\mathbf{u}_t(k|k)| \le \mathbf{u}_{t,max}$, $t \in \mathbb{Z}_{[0,m]}$, which is shown as (B4c). Note that

$$\max_{i\in[-h,0]}|\mathbf{u}_t(k+i|k)|^2 = \max_{i\in[-h,0]}\left|K_\mu\mathbf{y}(k+i|k)\right|^2 \le \max_{v\in\mathcal{V}}\left|K_\mu v\right|^2$$
$$= \max_{v\in\mathcal{V}}\left|\left(K_\mu\mathbf{X}_t^{-\frac{1}{2}}v\right)_t\right|^2 \le \left\|\left(K_\mu\mathbf{X}_t^{-\frac{1}{2}}\right)_t\right\|_2^2 = \left(K_\mu\mathbf{X}_t^{-1}K_\mu^T\right)_{tt} \tag{B14}$$

A sufficient condition for (B14) to hold is $(K_\mu\mathbf{X}_t^{-1}K_\mu^T)_{tt} \le \mathbf{u}_{t,max}^2$. As a result, (B14) can be guaranteed if there exists a matrix $\mathbf{Z}$ such that

$$\begin{bmatrix}\mathbf{Z} & K_\mu\\ K_\mu^T & \mathbf{X}_t^{-1}\end{bmatrix} \ge 0, Z_{tt} \le \mathbf{u}_{t,max}^2, \quad t \in \mathbb{Z}_{[0,m]} \tag{B15}$$

where $K_\mu = \sum_{b=1}^{L}\mathbf{Y}_b\mathbf{G}_b^{-1}$. A sufficient condition for (B15) so as to hold can be achieved.

$$\begin{bmatrix}\mathbf{Z} & \mathbf{Y}_b\mathbf{G}_b^{-1}\\ \left(\mathbf{Y}_b\mathbf{G}_b^{-1}\right)^T & \mathbf{X}_t^{-1}\end{bmatrix} \ge 0 \tag{B16}$$

By pre- and post-multiplying $\mathrm{diag}\{I, \mathbf{G}_b^T\}$ and then its transpose on both sides of (B16), we can obtain

$$\begin{bmatrix}\mathbf{Z} & \mathbf{Y}_b\\ \mathbf{Y}_b^T & \mathbf{G}_b^T\mathbf{X}_t^{-1}\mathbf{G}_b\end{bmatrix} \ge 0 \tag{B17}$$

Then inequality (B4c) can be easily be derived by applying inequality (B5) to (B17).

Theorem 3. *With the computed terminal constraint set Ω_t and the corresponding state feedback control law $\mathbf{u}(k) = K_\mu\mathbf{y}(k)$, the closed-loop system (16) is ISS with respect to disturbance $\mathbf{w}$.*

APPENDIX C

The communication delay is inherently unknown and random. In order to achieve sufficiently robust performance in the worst-case scenarios, we took the maximum value of time delays into account. In what follows, we aim to determine the maximum value of communication time delay. Toward this end, assume that the non-linear system (19) including time-varying delays can be written as follows:

$$\mathbf{y}(k+1) = \mathbf{A}_{0,\mu}\mathbf{y}(k) + \mathbf{A}_{h,\mu}\mathbf{y}(k-h) + \mathbf{B}_\mu\mathbf{u}(k) + \mathbf{E}_\mu\mathbf{w}(k) \tag{C1}$$

where $\mathbf{A}_{h,\mu} = \sum_{i=-h}^{-1}\mathbf{A}_{i,\mu}$. Note that $\mathbf{A}_{0,\mu}$ and $\mathbf{A}_{i,\mu}$ have aleardy been defined.

Theorem 4. *Suppose that there exist symmetric matrices $\mathbf{P}_t$, $\mathbf{S}_1 > 0$ and a scalar $\xi > 0$. If the following matrix inequality is feasible, the system (19) is asymptotically stable for all $i \in [-h, 0]$:*

$$\begin{bmatrix}(\mathbf{A}_{0,\mu}+\mathbf{A}_{h,\mu})^T\mathbf{P}_t + \mathbf{P}_t(\mathbf{A}_{0,\mu}+\mathbf{A}_{h,\mu}) + \xi\mathbf{P}_t & -h\mathbf{P}_t\mathbf{A}_{h,\mu}\mathbf{A}_{0,\mu} & -h\mathbf{P}_t\mathbf{A}_{h,\mu}^2\\ (-h\mathbf{P}_t\mathbf{A}_{h,\mu}\mathbf{A}_{0,\mu})^T & -\xi\mathbf{P}_t + \mathbf{S}_1 & 0\\ (-h\mathbf{P}_t\mathbf{A}_{h,\mu}^2)^T & 0 & -\mathbf{S}_1\end{bmatrix} \le 0 \tag{C2}$$

By solving the above matrix, the maximum value of time delay can be acquired

Proof. The proof of this theorem is so similar to Theorem 2.

17518695, 2022, 5, Downloaded from https://ietresearch.onlinelibrary.wiley.com/doi/10.1049/gtd2.12345 by Readcube (Labtiva Inc.), Wiley Online Library on [04/11/2022]. See the Terms and Conditions (https://onlinelibrary.wiley.com/terms-and-conditions) on Wiley Online Library for rules of use; OA articles are governed by the applicable Creative Commons License